Figure 1 Photographs of individuals with Coffin-Siris syndrome. The faces (left) and hypoplastic-to-absent nail of the fifth finger or toe (right) of affected individuals are shown with the color-coded names of the corresponding mutated genes. The green arrow indicates the absence of the distal phalanx in the fifth toe. No obvious hypoplastic nails were observed in subjects 12 or 19. Consent for all the photographs was obtained from the families of the affected individuals.

in mice[10]. However, in humans, abnormalities in both *SMARCA4* and *SMARCA2* are found in CSS, indicating that the in-frame partial deletion of the gene encoding BRM in subject 19 has a specific mutational effect different from that of simple inactivation in mice. These data support the idea that abnormalities in the BRG1-BAF and BRM-BAF complexes can cause the abnormal neurological development in CSS.

All the mutated genes found in CSS, except for *SMARCE1*, have been reported to be associated with tumorigenesis[1,2]. Among the 23 subjects with CSS, only subject 3 with an *ARID1A* mutation presented with hepatoblastoma. To our knowledge, haploinsufficiency and/or homozygous inactivation of *ARID1A* have been found in several types of cancer but not in hepatoblastoma. Malignancies were not detected in any of the other subjects with CSS examined here. It remains to be seen whether malignancies are robustly associated with CSS.

Given the fact that all the mutations in *ARID1A* and *ARID1B* in CSS were predicted to cause protein truncation, we proposed that haploinsufficiency of these two genes must be able to cause CSS. cDNA analysis of lymphoblastoid cell lines from subjects 1, 6 and 23 indicated that the mutated transcripts were subject to nonsense-mediated mRNA decay (**Supplementary Fig. 8**). In subject 10, the *ARID1B* mutation associated with the creation of a premature stop codon in the last exon did not result in nonsense-mediated mRNA decay as expected (**Supplementary Fig. 8**).

In regard to the other mutated genes, germline heterozygous truncation mutations in *SMARCB1* and *SMARCA4* have been reported

very likely to be deleterious (as it results in a truncated protein), the c.2144C>T mutation is likely to be a rare polymorphism. Of note, subject 12, who presented an atypical facial appearance and indistinct hypoplastic nails, had two interstitial deletions at 6q25.3–q27 involving *ARID1B*, as detected by a SNP array (**Supplementary Fig. 6** and **Supplementary Methods**). Furthermore, subject 14 was found to have an interstitial deletion of *SMARCA2* by a SNP array (**Supplementary Fig. 7** and **Supplementary Methods**). No other copy-number changes involving genes encoding SWI/SNF complex components were found in subjects 2, 14 or 18 by array analysis. The overall mutation detection rate was 87%. In total, 20 of the 23 subjects had a mutation affecting one of the six SWI/SNF subunits.

Mutations in CSS were identified in the BAF-specific subunits *ARID1A* and *ARID1B* but not in PBAF-specific subunits (*BRD7*, *ARID2* and *PBRM1*) (**Supplementary Table 3**). In addition, mutations were identified in *SMARCA4* (*BRG1*) as well as in *SMARCA2* (*BRM*) (**Supplementary Table 3**). The BRG1 and BRM proteins are mutually exclusive catalytic ATP subunits in mammalian SWI/SNF complexes. Of note, the majority of heterozygous *Smarca4*-null mice survive with susceptibility to neoplasia, with a minority dying after birth because of exencephaly, whereas homozygous *Smarca2*-null mice are viable and fertile[4]. In *Smarca2*-null mice, Brg1 is upregulated, suggesting that Brg1 can functionally replace Brm

Table 1 Mutations in individuals with Coffin-Siris syndrome

Subject ID	Gene	Mutation	Alteration	Type	Control allele frequency[a]
4	SMARCB1	c.1091_1093del AGA	p.Lys364del	De novo	0/502
11	SMARCB1	c.1130G>A	p.Arg377His	De novo	0/500
21	SMARCB1	c.1091_1093del AGA	p.Lys364del	NC	0/502
22	SMARCB1	c.1091_1093del AGA	p.Lys364del	NC	0/502
9	SMARCA4	c.1636_1638del AAG	p.Lys546del	De novo	0/350
7	SMARCA4	c.2576C>T	p.Thr859Met	De novo	0/368
5	SMARCA4	c.2653C>T	p.Arg885Cys	De novo	0/368
16	SMARCA4	c.2761C>T	p.Leu921Phe	De novo	0/368
25	SMARCA4	c.3032T>C	p.Met1011Thr	NC	0/372
17	SMARCA4	c.3469C>G	p.Arg1157Gly	De novo	0/368
19	SMARCA2	Partial deletion		De novo	–
24	SMARCE1	c.218A>G	p.Tyr73Cys	De novo	0/368
3	ARID1A	c.31_56del	p.Ser11Alafs*91	NC	0/330
6	ARID1A	c.2758C>T	p.Gln920*	NC	0/376
8	ARID1A	c.4003C>T	p.Arg1335*	De novo	–
1	ARID1B	c.1678_1688del	p.Ile560Glyfs*89	De novo	–
15	ARID1B	c.1903C>T	p.Gln635*	De novo	–
23	ARID1B	c.3304C>T	p.Arg1102*	De novo	–
10	ARID1B	c.2144C>T	p.Pro715Leu	NC	0/368
10	ARID1B	c.5632del G	p.Asp1878Metfs*96	NC	0/374
12	ARID1B	Microdeletion		NC	–

NC, not confirmed because parental samples were unavailable.
[a]The numbers indicate the observed allele frequency (alleles harboring the change/total tested alleles) in Japanese controls. None of the mutations was found in dbSNP132, the 1000 Genomes database or the National Heart, Lung, and Blood Institute (NHLBI) GO exomesequencing project database. –, not tested.

42

in individuals with rhabdoid tumor predisposition syndromes 1 (RTPS1; MIM 609322) and 2 (RTPS2; MIM 613325)[11,12], and various types of *SMARCB1* mutations (missense, in-frame deletion, nonsense and splice site) have been found in the germline of individuals with familial and sporadic schwannomatosis (MIM 162091)[13,14]. Furthermore, mice with heterozygous knockout of *Smarca4* or *Smarcb1* were prone to tumor development[2]. All the mutations in *SMARCA4* and *SMARCB1* in individuals with CSS were nontruncating (either missense or in-frame deletions), implying that they exert gain-of-function or dominant-negative effects (excluding haploinsufficiency as a cause). It is noteworthy that comparable germline mutations in *SMARCB1* have such different phenotypic consequences in their association with the phenotypes of CSS and schwannomatosis. The *SMARCB1* mutations in CSS and those in schwannomatosis are indeed different according to the Human Gene Mutation Database. With regard to the *SMARCA2* interstitial deletion in CSS, the change maintained the coding sequence reading frame but removed exons 20–27 that encode the HELICc domain. RT-PCR analysis confirmed the deletion of exons 20–27 at the cDNA level (**Supplementary Fig. 7**). These data suggest the importance of the HELICc domain in the SMARCA2 protein.

The various types of mutations in the genes encoding different SWI/SNF components resulted in similar CSS phenotypes. This suggests that the SWI/SNF complexes coordinately regulate chromatin structure and gene expression. This is the first report, to our knowledge, of germline mutations in SWI/SNF complex genes associated with a multiple congenital anomaly syndrome, highlighting new biological aspects of SWI/SNF complexes in humans. Similarly, genes encoding SNF2-related proteins, which are implicated as chromatin remodeling factors outside of SWI/SNF complexes, are mutated in different syndromes, including in α-thalassaemia/ mental retardation syndrome X-linked (ATRX; *ATRX* mutations) and in coloboma, heart defect, atresia choanae, retarded growth and development, genital abnormality and ear abnormality (CHARGE) syndrome (*CHD7* haploinsufficiency)[3]. We expect that more mutations affecting chromatin remodeling factors will be found in different human diseases.

URLs. Human Gene Mutation Database, https://portal.biobase-international.com/cgi-bin/portal/login.cgi.

1. Reisman, D., Glaros, S. & Thompson, E.A. *Oncogene* **28**, 1653–1668 (2009).
2. Wilson, B.G. & Roberts, C.W. *Nat. Rev. Cancer* **11**, 481–492 (2011).
3. Clapier, C.R. & Cairns, B.R. *Annu. Rev. Biochem.* **78**, 273–304 (2009).
4. Bultman, S. *et al. Mol. Cell* **6**, 1287–1295 (2000).
5. Hargreaves, D.C. & Crabtree, G.R. *Cell Res.* **21**, 396–420 (2011).
6. Xue, Y. *et al. Proc. Natl. Acad. Sci. USA* **97**, 13015–13020 (2000).
7. Coffin, G.S. & Siris, E. *Am. J. Dis. Child.* **119**, 433–439 (1970).
8. Bamshad, M.J. *et al. Nat. Rev. Genet.* **12**, 745–755 (2011).
9. Wittwer, C.T., Reed, G.H., Gundry, C.N., Vandersteen, J.G. & Pryor, R.J. *Clin. Chem.* **49**, 853–860 (2003).
10. Reyes, J.C. *et al. EMBO J.* **17**, 6979–6991 (1998).
11. Schneppenheim, R. *et al. Am. J. Hum. Genet.* **86**, 279–284 (2010).
12. Taylor, M.D. *et al. Am. J. Hum. Genet.* **66**, 1403–1406 (2000).
13. Boyd, C. *et al. Clin. Genet.* **74**, 358–366 (2008).
14. Hadfield, K.D. *et al. J. Med. Genet.* **45**, 332–339 (2008).

REPORT

De Novo and Inherited Mutations in COL4A2, Encoding the Type IV Collagen α2 Chain Cause Porencephaly

Yuriko Yoneda,[1] Kazuhiro Haginoya,[2,3] Hiroshi Arai,[4] Shigeo Yamaoka,[5] Yoshinori Tsurusaki,[1] Hiroshi Doi,[1] Noriko Miyake,[1] Kenji Yokochi,[6] Hitoshi Osaka,[7] Mitsuhiro Kato,[8] Naomichi Matsumoto,[1] and Hirotomo Saitsu[1],*

Porencephaly is a neurological disorder characterized by fluid-filled cysts or cavities in the brain that often cause hemiplegia. It has been suggested that porencephalic cavities result from focal cerebral degeneration involving hemorrhages. De novo or inherited heterozygous mutations in COL4A1, which encodes the type IV α1 collagen chain that is essential for structural integrity for vascular basement membranes, have been reported in individuals with porencephaly. Most mutations occurred at conserved Gly residues in the Gly-Xaa-Yaa repeats of the triple-helical domain, leading to alterations of the α1α1α2 heterotrimers. Here we report on two individuals with porencephaly caused by a heterozygous missense mutation in COL4A2, which encodes the type IV α2 collagen chain. Mutations c.3455G>A and c.3110G>A, one in each of the individuals, cause Gly residues in the Gly-Xaa-Yaa repeat to be substituted as p.Gly1152Asp and p.Gly1037Glu, respectively, probably resulting in alterations of the α1α1α2 heterotrimers. The c.3455G>A mutation was found in the proband's mother, who showed very mild monoparesis of the left upper extremity, and the maternal elder uncle, who had congenital hemiplegia. The maternal grandfather harboring the mutation is asymptomatic. The c.3110G>A mutation occurred de novo. Our study confirmed that abnormalities of the α1α1α2 heterotrimers of type IV collagen cause porencephaly and stresses the importance of screening for COL4A2 as well as for COL4A1.

Porencephaly (MIM 175780) is a neurological disorder characterized by fluid-filled cysts or cavities in the brain.[1] It has been suggested that porencephalic cysts are caused by a disturbance of vascular supply leading to cerebral degeneration.[2,3] Porencephaly clinically causes hemiplegia (most often), tetraplegia, epilepsy, and intellectual disability.[4,5] Monozygous twinning, maternal cardiac arrest or abdominal trauma, a deficient protein C anticoagulant pathway, or cytomegalovirus infections are risk factors for sporadic porencephaly.[2,6] Recently, mutations in the gene encoding type IV collagen α1 chain (COL4A1 [MIM 120130]) have been shown to cause familial porencephaly.[7] Since then, de novo and inherited COL4A1 mutations have been reported,[8–10] confirming that COL4A1 abnormalities are involved in both sporadic and familial porencephaly. Type IV collagens are basement membrane proteins that are expressed in all tissues including the vasculature. COL4A1 (α1 chain) and COL4A2 (α2 chain) are the most abundant type IV collagens, and form heterotrimers with 2:1 stoichiometry (α1α1α2).[11] A mouse model of the heterozygous COL4A1 mutation (Col4a1+/Δex40) showed cerebral hemorrhage and porencephaly and displayed abnormalities of vascular basement membranes, such as uneven edges, inconsistent density, and highly variable thickness.[7] In addition, a dominant negative effect of the Col4a1+/Δex40 mutation was demonstrated on collagen IV α1α1α2 heterotrimer assembly and its secretion.[7] In humans, most mutations are substitutions of the conserved Gly residue in the Gly-Xaa-Yaa repeat of the triple-helical domain, and they have a dominant negative effect on heterotrimer formation.[11,12]

COL4A2 (MIM 120090), which encodes the type IV α2 collagen chain, is a possible candidate for porencephaly because its mutations may affect the α1α1α2 heterotrimer. Supporting this idea, osteogenesis imperfecta type I-IV (MIM 166200, 166210, 259420, and 166220), which is characterized by abnormal bone fragility and low bone mass, is caused by mutations in both COL1A1 (MIM 120150) and COL1A2 (MIM 120160) that may interfere with formation of the collagen I α1α1α2 heterotrimer.[13] Moreover, mice lines harboring Col4a2 point mutations (Col4a2ENU415, c.227G>T [p.Val31Phe]; Col4a2ENU4003 and Col4a2ENU4020, c.2073G>A [p.Gly646Asp]) showed abnormalities of the lens, cornea, and vascular stability.[14] In the brains of the mutants, pseudocysts in the upper cortical plate, hemorrhages surrounding small blood vessels, and focal hemorrhagic necroses were observed, indicating that Col4a2 mutations cause abnormalities of the cerebral vasculature similar to those caused by Col4a1 mutations.[7,14] In this study, we screened for COL4A2 mutations in 35 Japanese individuals with porencephaly. Substitutions of a Gly residue in the Gly-Xaa-Yaa repeat were identified in two individuals (individuals 1 and 2). Clinical information and peripheral blood samples were

A

Family 1

B

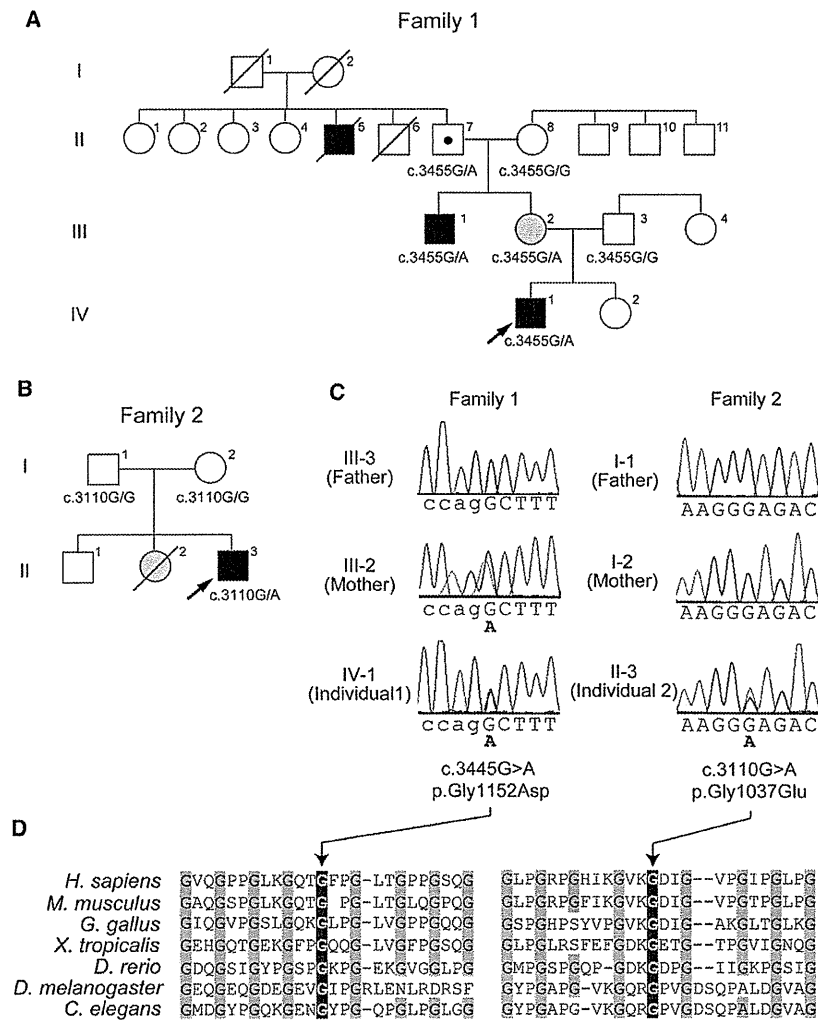Family 2

C

Family 1   Family 2

D

Figure 1. Pedigrees and COL4A2 Mutations in Individuals 1 and 2

Pedigrees of family 1(A) and family 2 (B). The arrows indicate the probands (Individual 1 in family 1 and individual 2 in family 2). The segregation of the COL4A2 mutations is shown. In family 1, the proband's mother (III-2) and maternal uncle (III-1) had mild monoparesis of the left upper extremity and congenital left hemiplegia and an assisted walk, respectively. The maternal grandfather (II-7) was healthy. The elder granduncle (II-5) was also afflicted by congenital hemiplegia and died in his 60s. (B) In family 2, the proband had a heterozygous mutation, but his parents did not have this mutation, indicating that the mutation occurred de novo. His elder sister (II-2) had intraventricular hemorrhage two days after birth but her DNA was unavailable.
(C) Electropherogram of family 1 (left) and family 2 (right). The intron and exon bases are in lower and upper cases, respectively. The c.3455G>A (p.Gly1152Asp) mutation in individual 1 was inherited from his mother. The c.3110G>A (p.Gly1037Glu) mutation in individual 2 occurred de novo.
(D) Multiple amino acid sequence alignments of COL4A2 proteins showing the evolutionarily conserved amino acids. The protein sequences obtained from the National Center for Biotechnology Information protein database are, NP_001837.2 (Homo sapiens), NP_034062.3 (Mus musculus), NP_001155862.1 (Gallus gallus), XP_002933063.1 (Xenopus tropicalis), XP_687811.5 (Danio rerio), AAB64082.1 (Drosophila melanogaster), and CAA80537.1 (Caenorhabditis elegans). The multiple sequence alignment was performed via the CLUSTALW website (see Web Resources). The positions of the conserved Gly residues in the Gly-X-Y repeats where the mutations occurred are highlighted with gray.

obtained from their family members after obtaining written informed consent. Experimental protocols were approved by the Institutional Review Board of Yokohama City University School of Medicine.

Individual 1 is 7 years old and a product of nonconsanguineous healthy parents (Figure 1A, arrow). There was no abdominal traumatism associated with the pregnancy and delivery in the mother. The individual was born at 36 weeks' gestation with a planned Caesarean section because, at 31 weeks' gestation, an antenatal ultrasound scan revealed an enlarged right lateral ventricle. Apgar scores were 9 at 1 min and 10 at 5 min. He weighed 2,900 g (+1.09 standard deviation [SD]) and had a head circumference of 32.5 cm (+0.05 SD). His early development was delayed with poor left hand use and abnormal leg movement. Brain magnetic resonance imaging (MRI) at 6 months showed an enlarged right lateral ventricle. Abrupt vomiting and nausea followed by motionless arrest

developed at the 10 months. An electroencephalogram (EEG) showed focal spikes in the right frontal region, and carbamazepine treatment was initiated at the 12 months. Rehabilitation was started at 10 months. The individual started rolling at 12 months, crawling at 18 months, and walking alone at 3 years. He had spastic triplegia (diplegia and left hemiplegia) showing hemiplegic and diplegic gait with fluent speech and normal word comprehension. At the 5 years of age, he underwent orthopedic surgery for foot deformity due to spastic paresis. An EEG showed spikes in the right occipital to posterior temporal region and midcentral region. A brain MRI at age 6 showed an enlarged right lateral ventricle, reduced volume of the right frontal white matter, and atrophic right cerebral peduncle and body of corpus callosum (Figures 2A–2C). His intelligent quotient [IQ] score, evaluated at 6 years with Wechsler Intelligence Scale for Children-Third Edition (WISC-III), was 74 (his performance IQ was 69 and his verbal IQ was
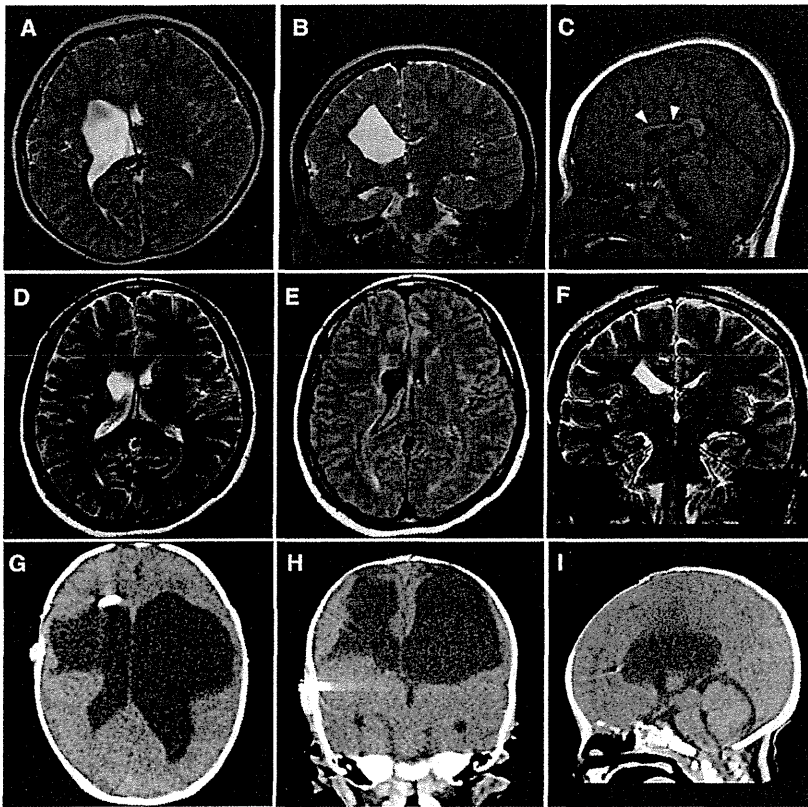
Figure 2. Brain Imaging in Individuals 1 and 2

(A–C) Brain MRIs of individual 1 at 6 years old; (A) T2-weighted axial image. (B) Coronal image. The images in (A) and (B) show an enlarged right lateral ventricle and a reduced volume of the right frontal white matter. (C) T1-weighted midline sagittal image showing atrophy of the body of the corpus callosum (arrowheads). The lesion responsible for the left leg paresis is not evident in these images.

(D–F) Brain MRIs of individual 1's mother at age 31. (D) T2-weighted axial and (F) coronal images show a mildly enlarged right lateral ventricle. (E) FLAIR axial image shows high signal intensity around the enlarged ventricular wall, which is consistent with mild porencephaly or periventricular venous infarction.

(G–I) CT images of individual 2 at 2 months of age. (G) Axial image. (H) Coronal image. (I) Sagittal image. The images in (G), (H), and (I) show an enlarged bilateral lateral ventricle and an extremely reduced volume of bilateral frontal white matter. The V-P shunt tube is also visible in the right lateral ventricle. The pontocerebellar structures seem to be normal.

82). The individual is now 7 years old and attending a local school. He can walk with ankle foot orthosis and hand assist. The epilepsy is well controlled with carbamazepine and clobazam. He does not show hematuria, muscular cramps, or ophthalmic abnormalities. His mother was born at term without asphyxia after an uneventful pregnancy. She had convulsions at the age of 18 months, and anticonvulsant was started under a diagnosis of focal epilepsy. Seizures were well controlled and treatment was discontinued at the age of 13. She first realized clumsiness of the left hand when she started learning piano and recorder at the age of 9. When she was a junior high school student, she felt severe headaches, and abnormal findings were pointed out in the brain MRI study (detailed information was unavailable). However, she did not undergo any more examinations because the headaches disappeared and did not recur. Neurological examination at 31 years revealed very mild monoparesis of the left upper extremity. She had neither spasticity nor exaggerated tendon reflexes. The grip power of her right and left hands was 25 and 15 kg, respectively. Mirror movement was observed on the right hand. The brain MRI revealed a mildly enlarged right lateral ventricle and high signal intensity around the enlarged ventricular wall on a Fluid Attenuated Inversion Recovery (FLAIR) image, which is consistent with mild porencephaly or periventricular venous infarction (Figures 2D–2F). MR angiography showed no aneurysms. Of note, his maternal elder uncle also showed congenital left hemiplegia with an assisted walk, and his maternal granduncle had also been afflicted by congenital hemiplegia, suggesting a genetic predisposition in the family (Figure 1A).

Individual 2 is 1 year and 4 months old and a product of nonconsanguineous healthy parents (Figure 1B, arrow). There was no abdominal traumatism associated with the pregnancy and delivery in the mother. He was born at 35 weeks' gestation. His birth weight was 1,694 g (-2.36 SD) and his head circumference was 29 cm (-1.77 SD). Mild asphyxia was observed, and he had Apgar scores of 3 at 1 min and 7 at 5 min. An ultrasound scan at 6 hr after birth revealed a parenchymal hemorrhage of the right cerebral hemisphere with an enlarged left lateral ventricle. Because a blood test revealed significant increases in prothrombin time (29.3 s) and activated partial thromboplastin time (104.3 s), but not in D-dimer (0.7 µg/ml) at 1 day after birth, he was treated with a daily infusion of fresh frozen plasma for 12 days. At 37 days after birth, he underwent a ventricular-peritoneal shunt (V-P shunt) operation for progressive enlargement of the lateral ventricle. Computed tomography (CT) at 2 months of age showed an enlarged bilateral lateral ventricle and an extremely reduced volume of bilateral frontal white matter (Figures 2G–2I). Blood coagulation was normalized at 7 months. At the 7 months, the individual did not show any head control or rolling, and presented with abnormal posturing and spastic quadriplegia dominant on the left side of his body. With

47

rehabilitation, he had full-range visual pursuit, a social smile, and incomplete head control. Although his spasticity improved, exaggerated deep tendon reflexes with synergic voluntary movement of the distal part of the extremities were recognized. An EEG at 1 year of age showed no epileptic discharges. His present developmental quotient is below 20. He did not show hematuria, muscular cramps, intracranial aneurysms, or cataracts. His elder sister was found to have an intraventricular hemorrhage two days after birth and underwent a V-P shunt. Her development was almost normal, and internal strabismus was noted. Unfortunately, she died in an accident at the age of four, and so her DNA was unavailable (Figure 1B).

Genomic DNA was isolated from peripheral blood leukocytes according to standard methods. DNA for mutation screening was amplified by illustra GenomiPhi V2 DNA Amplification Kit (GE Healthcare, Buckinghamshire, UK). The DNA of family members of individual 1 was isolated from saliva samples with Oragene (DNA Genotek Inc., Ontario, Canada). Exons 2 to 48 covering the entire COL4A2 coding region (GenBank accession number NM_001846.2) were examined by high-resolution melting curve (HRM) analysis or directly sequenced (for exon 46). The samples showing an aberrant melting curve pattern in the HRM analysis were sequenced. PCR primers and conditions are shown in Table S1, available online. All the mutations were verified with genomic DNA as a template. Two heterozygous mutations, c.3455G>A (p.Gly1152Asp) in individual 1 and c.3110G>A (p.Gly1037Glu) in individual 2, were identified. Both mutations occur at evolutionary conserved Gly residues in the Gly-X-Y repeats (Figure 1D), suggesting that the two mutations may alter the collagen IV α1α1α2 heterotrimers. These mutations were absent in 200 normal Japanese controls, and our evaluation with web-based prediction tools strongly suggested that these substitutions are pathogenic (Table S2). Screening for COL4A1 mutations was negative for both individuals (data not shown). The c.3455G>A mutation was found in the proband's mother and the maternal uncle, who showed very mild monoparesis of the left upper extremity and congenital left hemiplegia, respectively, and in maternal grandfather who is asymptomatic (Figures 1A and 1B). Therefore the c.3455G>A mutation can be considered as a pathogenic mutation with incomplete penetrance. The c.3110G>A mutation in individual 2 was not found in his parents, indicating that this mutation occurred de novo (Figure 1C).

Here we report two individuals with porencephaly who harbor COL4A2 mutations. In individual 2, the mutation occurred de novo. It is noteworthy that individual 2's elder sister also suffered from an intraventricular hemorrhage. A coincidental phenocopy in the sister is possible and would be consistent with de novo occurrence of the mutation. Alternatively, the sister might have the same mutation, which could be inherited from either one of the parents with a germline-mosaic mutation, though it was impossible to examine the sister because her sample is unavailable.

Thus, with the present data, we concluded that the c.3110G>A mutation occurred de novo. On the other hand, the mutation in individual 1 was inherited from his mildly affected mother. In addition, congenital hemiplegia is observed in familial members of individual 1; the segregation of the c.3455G>A mutation is consistent with a dominant trait with incomplete penetrance. Such incomplete penetrance also has been reported in familial porencephalies with COL4A1 mutations,[8,9] suggesting that abnormalities of collagen IV α1α1α2 heterotrimers may conspire with other risk factors. The porencephalic cyst was unilateral in individual 1 and bilateral in individual 2, who required shunting, indicating variable severities caused by the different COL4A2 mutations. Most porencephalic cysts caused by COL4A1 mutations are unilateral;[9] however, Meuwissen et al. recently reported de novo COL4A1 mutations in sporadic extensive bilateral porencephaly resembling hydranencephaly, indicating similar variable severities caused by COL4A1 mutations.[10] Thus the involvement of COL4A1 and COL4A2 abnormalities should be considered in porencephaly and related pre- and perinatal cerebral hemorrhages, regardless of their severities.

It has been reported that COL4A1 mutations cause a variety of phenotypes, including porencephaly, infantile hemiplegia, and cerebral small vessel diseases involving both ischemic stroke and intracerebral hemorrhage with radiological features of lacunar infarction, and leukoaraiosis in adult individuals.[9,15–18] The phenotypes in the central nervous system are often accompanied by ocular features (cataracts, retinal vessel tortuosity and hemorrhage, and defects of the anterior segment of the eye), nephropathy, and muscle cramps.[9,16,17] Considering the common pathological mechanism between COL4A1 and COL4A2 mutations (abnormalities of collagen IV α1α1α2 heterotrimers), COL4A2 mutations also may be involved in small vessel diseases that can be manifested in adulthood. Supporting this idea, mice lines harboring Col4a2 point mutations showed cataracts, abnormalities of the lens and the cornea, and cerebral abnormalities.[14] Thus it is important to identify mutations in both COL4A1 and COL4A2 in individuals with porencephaly as well as in asymptomatic carriers, for whom the prevention of stroke and genetic counseling are quite important. Identification of pathogenic mutations in individuals with porencephaly is of great interest for obstetricians and pediatricians, and for neurologists working for adult individuals.

In summary, we have identified mutations in COL4A2 as a genetic cause of both sporadic and familial porencephaly. Our data further support the importance of genetic testing in porencephaly and related pre- and perinatal cerebral hemorrhages for which the genetic predisposition is gradually being uncovered.

Supplemental Data

48

Web Resources

The URLs for data presented herein are as follows:

Clustal W, http://www.genome.jp/tools/clustalw/
GenBank, http://www.ncbi.nlm.nih.gov/Genbank/
Online Mendelian Inheritance in Man (OMIM), http://www.omim.org

References

1. Berg, R.A., Aleck, K.A., and Kaplan, A.M. (1983). Familial porencephaly. Arch. Neurol. *40*, 567–569.
2. Govaert, P. (2009). Prenatal stroke. Semin. Fetal Neonatal Med. *14*, 250–266.
3. Hunter, A. (2006). Porencephaly. In Human Malformations and related Anomalies, S. Re and H. Jg, eds. (New York: Oxford University Press), pp. 645–654.
4. Mancini, G.M., de Coo, I.F., Lequin, M.H., and Arts, W.F. (2004). Hereditary porencephaly: clinical and MRI findings in two Dutch families. Eur. J. Paediatr. Neurol. *8*, 45–54.
5. Vilain, C., Van Regemorter, N., Verloes, A., David, P., and Van Bogaert, P. (2002). Neuroimaging fails to identify asymptomatic carriers of familial porencephaly. Am. J. Med. Genet. *112*, 198–202.
6. Moinuddin, A., McKinstry, R.C., Martin, K.A., and Neil, J.J. (2003). Intracranial hemorrhage progressing to porencephaly as a result of congenitally acquired cytomegalovirus infection—an illustrative report. Prenat. Diagn. *23*, 797–800.
7. Gould, D.B., Phalan, F.C., Breedveld, G.J., van Mil, S.E., Smith, R.S., Schimenti, J.C., Aguglia, U., van der Knaap, M.S., Heutink, P., and John, S.W. (2005). Mutations in *Col4a1* cause perinatal cerebral hemorrhage and porencephaly. Science *308*, 1167–1171.
8. Breedveld, G., de Coo, I.F., Lequin, M.H., Arts, W.F., Heutink, P., Gould, D.B., John, S.W., Oostra, B., and Mancini, G.M. (2006). Novel mutations in three families confirm a major role of *COL4A1* in hereditary porencephaly. J. Med. Genet. *43*, 490–495.
9. Lanfranconi, S., and Markus, H.S. (2010). *COL4A1* mutations as a monogenic cause of cerebral small vessel disease: a systematic review. Stroke *41*, e513–e518.
10. Meuwissen, M.E., de Vries, L.S., Verbeek, H.A., Lequin, M.H., Govaert, P.P., Schot, R., Cowan, F.M., Hennekam, R., Rizzu, P., Verheijen, F.W., et al. (2011). Sporadic *COL4A1* mutations with extensive prenatal porencephaly resembling hydranencephaly. Neurology *76*, 844–846.
11. Khoshnoodi, J., Pedchenko, V., and Hudson, B.G. (2008). Mammalian collagen IV. Microsc. Res. Tech. *71*, 357–370.
12. Engel, J., and Prockop, D.J. (1991). The zipper-like folding of collagen triple helices and the effects of mutations that disrupt the zipper. Annu. Rev. Biophys. Biophys. Chem. *20*, 137–152.
13. Gajko-Galicka, A. (2002). Mutations in type I collagen genes resulting in osteogenesis imperfecta in humans. Acta Biochim. Pol. *49*, 433–441.
14. Favor, J., Gloeckner, C.J., Janik, D., Klempt, M., Neuhäuser-Klaus, A., Pretsch, W., Schmahl, W., and Quintanilla-Fend, L. (2007). Type IV procollagen missense mutations associated with defects of the eye, vascular stability, the brain, kidney function and embryonic or postnatal viability in the mouse, Mus musculus: an extension of the *Col4a1* allelic series and the identification of the first two *Col4a2* mutant alleles. Genetics *175*, 725–736.
15. Vahedi, K., and Alamowitch, S. (2011). Clinical spectrum of type IV collagen (COL4A1) mutations: a novel genetic multisystem disease. Curr. Opin. Neurol. *24*, 63–68.
16. Sibon, I., Coupry, I., Menegon, P., Bouchet, J.P., Gorry, P., Burgelin, I., Calvas, P., Orignac, I., Dousset, V., Lacombe, D., et al. (2007). *COL4A1* mutation in Axenfeld-Rieger anomaly with leukoencephalopathy and stroke. Ann. Neurol. *62*, 177–184.
17. Alamowitch, S., Plaisier, E., Favrole, P., Prost, C., Chen, Z., Van Agtmael, T., Marro, B., and Ronco, P. (2009). Cerebrovascular disease related to *COL4A1* mutations in HANAC syndrome. Neurology *73*, 1873–1882.
18. Gould, D.B., Phalan, F.C., van Mil, S.E., Sundberg, J.P., Vahedi, K., Massin, P., Bousser, M.G., Heutink, P., Miner, J.H., Tournier-Lasserve, E., and John, S.W. (2006). Role of COL4A1 in small-vessel disease and hemorrhagic stroke. N. Engl. J. Med. *354*, 1489–1496.

ORIGINAL ARTICLE

Missense mutations in the DNA-binding/dimerization domain of *NFIX* cause Sotos-like features

Yuriko Yoneda[1], Hirotomo Saitsu[1], Mayumi Touyama[2], Yoshio Makita[3], Akie Miyamoto[4], Keisuke Hamada[5], Naohiro Kurotaki[6], Hiroaki Tomita[7], Kiyomi Nishiyama[1], Yoshinori Tsurusaki[1], Hiroshi Doi[1], Noriko Miyake[1], Kazuhiro Ogata[5], Kenji Naritomi[8] and Naomichi Matsumoto[1]

Sotos syndrome is characterized by prenatal and postnatal overgrowth, characteristic craniofacial features and mental retardation. Haploinsufficiency of *NSD1* causes Sotos syndrome. Recently, two microdeletions encompassing *Nuclear Factor I-X (NFIX)* and a nonsense mutation in *NFIX* have been found in three individuals with Sotos-like overgrowth features, suggesting possible involvements of *NFIX* abnormalities in Sotos-like features. Interestingly, seven frameshift and two splice site mutations in *NFIX* have also been found in nine individuals with Marshall–Smith syndrome. In this study, 48 individuals who were suspected as Sotos syndrome but showing no *NSD1* abnormalities were examined for *NFIX* mutations by high-resolution melt analysis. We identified two heterozygous missense mutations in the DNA-binding/dimerization domain of the NFIX protein. Both mutations occurred at evolutionally conserved amino acids. The c.179T>C (p.Leu60Pro) mutation occurred *de novo* and the c.362G>C (p.Arg121Pro) mutation was inherited from possibly affected mother. Both mutations were absent in 250 healthy Japanese controls. Our study revealed that missense mutations in *NFIX* were able to cause Sotos-like features. Mutations in DNA-binding/dimerization domain of NFIX protein also suggest that the transcriptional regulation is abnormally fluctuated because of *NFIX* abnormalities. In individuals with Sotos-like features unrelated to *NSD1* changes, genetic testing of *NFIX* should be considered.
Journal of Human Genetics advance online publication, 2 February 2012; doi:10.1038/jhg.2012.7

Keywords: DNA-binding/dimerization domain; missense mutation; *NFIX*; Sotos syndrome

INTRODUCTION

Sotos syndrome (MIM #117550) is an overgrowth syndrome characterized by tall stature and/or macrocephaly, distinctive facial appearance and mental retardation.[1] A *de novo* t(5;8)(q35;q24.1) translocation in a patient with Sotos syndrome revealed disruption of *NSD1* at 5q35. Subsequent identification of nonsense, frameshift and submicroscopic deletion mutations of *NSD1* in patients with Sotos syndrome clearly showed that haploinsufficiency of *NSD1* causes Sotos syndrome.[2] *NSD1* encodes nuclear receptor-binding SET domain protein 1, which functions as a histone methyltransferase that activates and represses transcription through chromatin modification.[3] The diagnosis of Sotos syndrome is established by confirming *NSD1* abnormalities,[4] and abnormalities of *NSD1* causes up to 90% of Sotos syndrome cases. However, a part of patients with suspected Sotos syndrome are known to show no abnormalities in *NSD1*,[5] suggesting involvement of another gene.

Recently it was reported that two patients with Sotos-like overgrowth features possessed microdeletions encompassing *Nuclear Factor I-X (NFIX)* at 19p13.2. In addition, a nonsense mutation in *NFIX* was identified in one patient with Sotos-like features.[6] Interestingly, frameshift and donor-splice site mutations were also identified in Marshall–Smith syndrome (MIM 602535) that is osteochondysplasia syndrome characterized by accelerated skeletal maturation, relative failure to thrive, respiratory difficulties, mental retardation and unusual facial features.[7] Therefore, *NFIX* mutations could cause either Sotos-like features or Marshall–Smith syndrome. Whereas the transcripts possessing the nonsense mutation in a patient with Sotos-like features suffered from the nonsense-mediated mRNA decay, transcripts of mutated alleles (by a donor-spice site and two frameshift mutations) in patients with Marshall–Smith syndrome escaped from the nonsense-mediated mRNA decay surveillance and could be translated, suggesting that haploinsufficiency of *NFIX* leads to

[1]Department of Human Genetics, Yokohama City University Graduate School of Medicine, Yokohama, Japan; [2]Department of Pediatrics, Okinawa Child Development Center, Okinawa, Japan; [3]Education Center, Asahikawa Medical University, Asahikawa, Japan; [4]Department of Pediatrics, Hokkaido Asahikawa Habilitation Center for Disabled Children, Asahikawa, Japan; [5]Department of Biochemistry, Yokohama City University Graduate School of Medicine, Yokohama, Japan; [6]Department of Neuropsychiatry, Nagasaki University Graduate School of Biomedical Sciences, Nagasaki, Japan; [7]Department of Biological Psychiatry, Tohoku University Graduate School of Medicine, Sendai, Japan and [8]Department of Medical Genetics, University of the Ryukyus Faculty of Medicine, Nishihara, Japan
Correspondence: Dr N Matsumoto, Department of Human Genetics, Yokohama City University Graduate School of Medicine, Fukuura 3-9, Kanazawa-ku, Yokohama 236-0004, Japan.
E-mail: naomat@yokohama-cu.ac.jp
Received 9 September 2011; revised 21 November 2011; accepted 5 January 2012

Sotos-like features and dominant-negative effects of the truncated NFIX proteins cause Marshall–Smith syndrome.[6]

In this study, we screened for *NFIX* mutations in 48 Japanese patients who were suspected as Sotos syndrome, but showed neither deletions nor mutations in *NSD1*. Detailed genetic and clinical data are presented.

MATERIALS AND METHODS

Subjects

A total of 48 patients suspected as Sotos syndrome were analyzed for *NFIX* mutations. *NSD1* investigation by sequencing and fluorescent *in situ* hybridization analysis was negative in these patients. In this study, the patients presenting with cardinal features of Sotos syndrome (specific craniofacial features, intellectual disability and overgrowth to same extent) but showing no *NSD1* abnormalities are referred as those with 'Sotos-like features'. Experimental protocols were approved by the Committee for Ethical issues at Yokohama City University School of Medicine. All individuals were investigated in agreement with the requirements of Japanese regulations.

Mutation analysis

Genomic DNA was isolated from peripheral blood leukocytes according to standard methods. DNA for mutation screening was amplified by illustra GenomiPhi V2 DNA Amplification Kit (GE Healthcare, Buckinghamshire, UK). Sequencing of exon 1 and high-resolution melting curve (HRM) analysis of exon 2–9 covering the *NFIX* coding region (GenBank accession number NM_002501.2) were performed. For exon 1, the 12 μl PCR mixture contained 30 ng DNA, 0.3 μM each primer, 0.4 mM each dNTP, 1× PCR buffer for KOD FX and 0.3 U KOD FX polymerase (Toyobo, Osaka, Japan). For exons 2–9, real-time PCR and HRM analysis were serially performed in 12 μl mixture on Rotor-Gene Q (QIAGEN, Hilden, Germany). For exon 7, the PCR mixture contained 30 ng DNA, 0.3 μM each primer, 0.4 mM each dNTP, 0.36 μl SYTO9 (Invitrogen, Carlsbad, CA, USA), 0.4 mM each dNTP, 1× PCR buffer for KOD FX and 0.3 U KOD FX polymerase (Toyobo). For the remaining exons, the PCR mixture contained 30 ng DNA, 0.25 μM each primer, 0.36 μl SYTO9 (Invitrogen), 0.2 mM each dNTP, 1× ExTaq buffer and 0.375 U ExTaq HS (Takara, Otsu, Japan). Primers and conditions of PCR are shown in Supplementary Table 1. The PCR products showing an aberrant melting curve were sequenced. All the novel mutations in DNA amplified by GenomiPhi were verified by sequencing of PCR products using genomic DNA as a template. Mutations were checked in 250 Japanese normal controls (500 alleles) by HRM analysis.

Parentage testing

For the family showing *de novo* mutations, parentage was confirmed by microsatellite analysis as previously described.[8] Biological parentage was judged if more than four informative markers were compatible and other uninformative markers showed no discrepancies.

Prediction of functional effect

The effect of the mutations for protein features was predicted by following web-based prediction tools: SIFT (http://sift.jcvi.org/), PolyPhen (http://genetics.bwh.harvard.edu/pph/), PolyPhen-2 (http://genetics.bwh.harvard.edu/pph2/), Mutation Taster (http://www.mutationtaster.org/) and Align GVGD (http://agvgd.iarc.fr/agvgd_input.php).

RESULTS

NFIX mutations

Two heterozygous missense mutations were identified. The c.179T>C (p.Leu60Pro) mutation in patient 1 were not found in her parents, indicating that the mutation occurred *de novo* (Figure 1a). Biological parentage was confirmed by several microsatellite markers (data not shown). The c.362G>C (p.Arg121Pro) mutation in patient 2 was found in his mother (Figure 1a). These two mutations occurred at evolutionary conserved amino acids (Figure 1b) and were absent in 250 Japanese normal controls. Interestingly, the missense changes were

located in DNA-binding/dimerization domain of the NFIX protein (Figure 1c). Evaluation with web-based prediction tools strongly suggested that these substitutions are pathogenic (Supplementary Table 2).

Clinical information of the patients

Patient 1 is a product of unrelated healthy parents. The body weight at birth was 2816 g (−0.6 s.d.), height 48.8 cm (0 s.d.) and OFC 33.5 cm (+0.3 s.d.). Neonatal hypotonia was recognized. At 17 months of age, her weight was 9.24 kg (−0.5 s.d.), height 84.9 cm (+2 s.d.) and OFC 48 cm (+1.2 s.d.). The facial appearance showed long/narrow and triangular face, high forehead, midface hypoplasia, prominent ears, epicanthal folds, strabismus, down-slanting palpebral fissures, short nose with anteverted nares, prominent long philtrum, everted lower lip and narrow palate (Figure 1d). Large hands/feet, prominent fingertips, pectus excavatum were also noted. Her primary dentition started at 7 months of age and was completed by 17 months of age. Bone age was estimated as 3 years at 17 months of age and as 5 years at 3 years of age. Bullet-shaped phalanges, which are typical features of Marshall–Smith syndrome, were not observed. She was initially diagnosed as Sotos syndrome. She showed mental retardation and severe developmental delay with developmental quotients of 19. Scoliosis was noted at 18 months of age and surgically treated for several times. Complex partial seizures were noted at 4 years of age and were controlled with phenytoin and zonisamide. At present (17 years of age), prognathia was observed (Figure 1e). Her weight was 40 kg (−2 s.d.) and height 156.5 cm (−0.2 s.d.).

Patient 2 is a male at age of 20 years. The birth weight was 2938 g (−0.4 s.d.), height 51 cm (+0.8 s.d.) and OFC 35.5 cm (+1.4 s.d.). Respiratory insufficiency was noted, but no visceral malformations were pointed out. Bilateral tubing therapy was performed for recurrent bilateral exudative otitis media at 4 years of age. At 14 years of age, his weight was 58.1 kg (+0.6 s.d.) and height 185.7 cm (+3.5 s.d.). Mental retardation was evident as the IQ score (Tanaka–Binet intelligence test) was 59. Craniofacial features included high forehead, down-slanting palpebral fissures and prognathia. He was suspected as Sotos syndrome. His mother showed tall stature, suggesting that c.362G>C led to overgrowth in the mother. Unfortunately, further details of clinical features in the mother are unavailable. Clinical information of two patients is summarized in Table 1.

DISCUSSION

NFIX is a member of the nuclear factor I (NFI) family proteins, which are implicated as site-specific DNA-binding proteins known to function in viral DNA replication and gene expression regulation.[9] NFI proteins form homo- or heterodimers and bind to the palindromic DNA consensus sequence through its N-terminal DNA-binding/dimerization domain.[10] Point mutations in DNA-binding/dimerization domain of NFI protein have been shown to cause loss of dimerization, DNA-binding and replication activities,[11] highlighting the importance of structural integrity of DNA-binding/dimerization domain. It has been reported that the DNA binding domain of SMADs and NFI transcription factors shared considerable structural similarity, and the secondary structure of the DNA-binding domain of NFI was estimated based on that of SMADs.[12] In this study, we identified two heterozygous missense mutations, the c.179T>C (p.Leu60Pro) and the c.362G>C (p.Arg121Pro), in the DNA-binding/dimerization domain. Of note, two mutations are estimated to be localized within α-helical region of DNA-binding domain and at evolutionally conserved amino acids between SMADs and NFI.[12] In addition, two mutations cause substitutions to a proline residue,
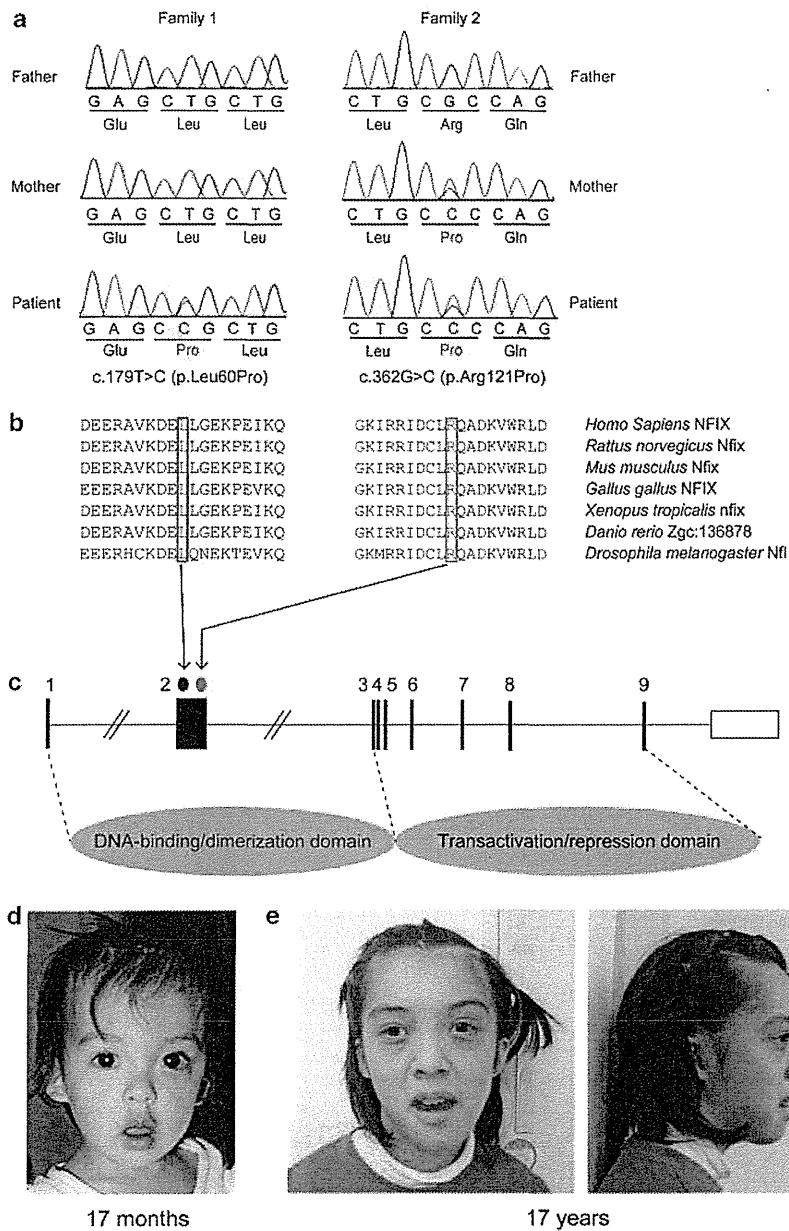
Figure 1 Missense mutations in *NFIX* in individuals with Sotos-like features. (a) Electropherogram of family 1 (left) and family 2 (right). The c.179T>C (p.Leu60Pro) mutation occured *de novo*. The c.362G>C (p.Arg121Pro) mutation was inherited from his mother. (b) An amino-acid sequence alignments of NFIX protein including amino-acid positions 60 and 121. Protein sequences were obtained through the NCBI protein database and multiple sequence alignment was performed by CLUSTALW web site (http://clustalw.ddbj.nig.ac.jp/). (c) Schematic representation of *NFIX* consisting of nine exons. UTR and coding exons are indicated by open and filled rectangles, respectively. The location of mutations is indicated by red (c.179T>C) and blue (c.362G>C) dots. At the bottom, C-terminal DNA-binding/dimerization domain and N-terminal transactivation/repression domain are depicted. Both the c.179T>C and c.362G>C mutations are located in exon 2 encoding a part of DNA-binding/dimerization domain. (d) Facial appearance of patient 1 at 17 months of age, showing long/narrow and triangular face, down slanting, short nose with anteverted nares and everted lower lip. (e) At 17 years of age, prognathia was noted in patient 1.

which is a unique amino acid characterized by imino radical. Proline has a pyrrolidine ring that restricts the available conformational space; therefore, it has effects on chain conformation and the process of protein folding.[13] Thus, it is very likely that two mutations could affect DNA-binding activity of NFIX protein through conformational changes of the DNA-binding domain.

Because *NFIX* mutations could cause both Marshall–Smith syndrome and Sotos-like features,[6] it is great concern to which of them two patients with missense mutations could be classified. Main clinical features of Sotos syndrome are childhood overgrowth including tall stature and/or macrocephaly, characteristic face and mental retardation. Other minor features are scoliosis, hypotonia in infancy, seizures,

Table 1 Clinical features of two patients with missense mutations in *NFIX*

Genetics	NFIX deletion/mutation	Patient 1 c.179T>C	Patient 2 c.362G>C	Reported by Malan et al.[6] Patient A del 19p13.3	Patient B del 19p13.3	Patient C c.568C>T
Epidemiology	Age at last evaluation (years)	17	14	14	10	27
	Sex	F	M	M	M	F
	Mat/pat age	48/52	?/?	31/33	25/30	31/31
Prenatal growth	Birth weight (g)	2816 (−0.6 s.d.)	2938 (−0.4 s.d.)	4500 (>95)	3110 (10–50)	3600 (50–90)
	Birth height (cm)	48.8 (0 s.d.)	51 (+0.8 s.d.)	53 (95)	49 (50)	52 (95)
	OFC (cm)	33.5 (+0.3 s.d.)	35.5 (+1.4 s.d.)	38 (>95)	33.5 (10)	37.5 (>95)
Postnatal growth	Weight (kg)	9.24 (−0.5 s.d.)[a]	58.1 (+0.6 s.d.)[b]	>P98	>P98	>P98
	Height (cm)	84.9 (+2 s.d.)[a]	185.7 (+3.5 s.d.)[b]	>P98	>P98	>P98
Development						
SS	Autistic traits	−	−	+	+	+
	Behavioral anomalies	NA	−	+	+	+
	Motor retardation	+	+	+	−	−
	Hypotonia	+	+	+	+	−
Overlapped	Mental retardation	+	+	+	+	+
	Degree of delay	DQ19	IQ42	NA	NA	NA
	Speech delay	+	+	+	+	+
	First words (months)	24	18	NA	NA	NA
Craniofacial features						
SS	Long/narrow face	+	−	+	+	+
	Down-slanting palpebral fissures	+	+	+	−	+
	Small mouth	NA	−	+	−	+
	Prognathia	+	+	+	−	−
Overlapped	High forehead	+	+	+	+	+
MSS	Everted lower lip	+	−	+	−	+
	Underdeveloped midface	+	−	NA	NA	NA
	Proptosis	NA	−	NA	NA	NA
	Short nose	+	−	NA	NA	NA
	Prominent premaxilla	NA	−	NA	NA	NA
	Gum hypertrophy	+[c]	−	NA	NA	NA
	Retrognathia	−	−	NA	NA	NA
Eyes						
SS	Hypermotropia	−	−	+	+	−
	Strabismus	+	−	+	−	+
	Nystagmus	−	−	−	−	+
	Astigmatism	NA	NA	−	+	−
MSS	Myopia	NA	−	NA	NA	NA
	Blue sclerae	NA	−	NA	NA	NA
Musculo-skeletal abnormalities						
SS	Abdominal wall hypotonia	−	−	+	−	+
	Pectus excavatum	+	−	+	+	−
	Coxa valga	−	−	+	+	−
Overlapped	Scoliosis	+	−	+	−	+
	Advanced bone age	+	NA	+	+	+
MSS	Abnormal bone maturation	NA	NA	NA	NA	NA
	Bone fractures	−	−	NA	NA	NA
	Kyphosis	−	−	NA	NA	NA
	Umbilical hernia	−	−	NA	NA	NA

Abbreviations: F, female; M, male; Mat/pat, maternal/paternal; MSS, Marshall–Smith syndrome; NA, not ascertained; OFC, Occipitofrontal circumference; SS, Sotot's syndrome.
Growth of patients 1 and 2 is indicated with s.d. and that of patients in the report of Malan *et al.*[6] is indicated with percentile.
[a]At 17 months.
[b]At 14 years.
[c]Suggested the possibility of the adverse drug reaction.

cardiac defect and genitourinary anomalies.[5] On the other hand, main clinical features of Marshall–Smith syndrome are moderate to severe developmental delay with absent or limited speech, unusual behavior, disharmonic bone maturation, respiratory compromise secondary to upper airway obstruction, short stature and kyphoscoliosis.[14] One of remarkable differences between Sotos syndrome and Marshall–Smith syndrome is facial appearances. Although both syndromes has high forehead, Sotos syndrome has a long/narrow face, triangular shaped face with a prominent chin, down-slanting of the palpebral fissures,[1,4–5] whereas Marshall–Smith syndrome has proptosis, under-developed midface and prominent premaxilla.[7,14] In patient 1, although some characteristic features of Marshall–Smith syndrome such as everted lower lip, short nose and midface hypoplasia were observed, overall facial appearance, overgrowth features at 17 month of age, scoliosis, hypotonia and seizures were consistent with Sotos syndrome. Similarly, in patient 2, the facial appearance, tall stature and macrocephaly were consistent with Sotos syndrome. In both patients, their body weights were relatively low in comparison with their heights. This is consistent with the fact that, throughout childhood and early adolescence, the height was usually more significantly increased than weight in Sotos patients.[15] In addition, our patients did not show respiratory difficulties, one of specific features in Marshall–Smith syndrome, which cause early death in the neonatal period or early infancy.[7] Thus missense mutations in the DNA-binding/dimerization domain, which may lead to loss of transcriptional regulation by NFIX protein, could cause Sotos-like syndrome in two patients.

Many clinical features including tall statue, mental retardation, speech delay and high forehead are shared between our patients and three patients reported by Malan et al.[6] with NFIX abnormalities. The recognizable difference is autistic traits. Autistic traits are not observed in our patients but all of Malan et al's[6] patients. Thus there is a possibility that autistic traits are caused by haploinsufficiency of NFIX in Malan et al's[6] patients, but not by misssense mutations in the DNA-binding/dimerization domain. However, identification of a greater number of cases with NFIX mutations is required to confirm this hypothesis.

In conclusion, our report provides further evidences that NFIX is a causative gene for Sotos-like features. Abnormalities of NSD1 are found in majority of Sotos syndrome cases and aberration of other genes including NFIX may be found in the minority of Sotos syndrome/Sotos-like features. Genetic testing of NFIX should be considered in such patients if no NSD1 abnormalities were identified.

CONFLICT OF INTEREST

The authors declare no conflict of interest.

1 Leventopoulos, G., Kitsiou-Tzeli, S., Kritikos, K., Psoni, S., Mavrou, A., Kanavakis, E. et al. A clinical study of Sotos syndrome patients with review of the literature. Pediatr. Neurol. 40, 357–364 (2009).
2 Kurotaki, N., Imaizumi, K., Harada, N., Masuno, M., Kondoh, T., Nagai, T. et al. Haploinsufficiency of NSD1 causes Sotos syndrome. Nat. Genet. 30, 365–366 (2002).
3 Rayasam, G. V., Wendling, O., Angrand, P. O., Mark, M., Niederreither, K., Song, L. et al. NSD1 is essential for early post-implantation development and has a catalytically active SET domain. EMBO J. 22, 3153–3163 (2003).
4 Visser, R. & Matsumoto, N. in Inborn Errors of Development (eds Epstein, C. J., Erickson, R. P., Wynshaw-Boris, A.) 1032–1037 (Oxford University Press, New York, 2008).
5 Tatton-Brown, K. & Rahman, N. Sotos syndrome. Eur. J. Hum. Genet. 15, 264–271 (2007).
6 Malan, V., Rajan, D., Thomas, S., Shaw, A. C., Louis Dit Picard, H., Layet, V. et al. Distinct effects of allelic NFIX mutations on nonsense-mediated mRNA decay engender either a Sotos-like or a Marshall-Smith syndrome. Am. J. Hum. Genet. 87, 189–198 (2010).
7 Adam, M. P., Hennekam, R. C., Keppen, L. D., Bull, M. J., Clericuzio, C. L., Burke, L. W. et al. Marshall-Smith syndrome: natural history and evidence of an osteochondrodys-plasia with connective tissue abnormalities. Am. J. Med. Genet. A. 137, 117–124 (2005).
8 Saitsu, H., Kato, M., Mizuguchi, T., Hamada, K., Osaka, H., Tohyama, J. et al. De novo mutations in the gene encoding STXBP1 (MUNC18-1) cause early infantile epileptic encephalopathy. Nat. Genet. 40, 782–788 (2008).
9 Gronostajski, R. M. Roles of the NFI/CTF gene family in transcription and development. Gene 249, 31–45 (2000).
10 Kruse, U. & Sippel, A. E. Transcription factor nuclear factor I proteins form stable homo- and heterodimers. FEBS Lett. 348, 46–50 (1994).
11 Armentero, M. T., Horwitz, M. & Mermod, N. Targeting of DNA polymerase to the adenovirus origin of DNA replication by interaction with nuclear factor I. Proc. Natl. Acad. Sci. USA 91, 11537–11541 (1994).
12 Stefancsik, R. & Sarkar, S. Relationship between the DNA binding domains of SMAD and NFI/CTF transcription factors defines a new superfamily of genes. DNA Seq. 14, 233–239 (2003).
13 MacArthur, M. W. & Thornton, J. M. Influence of proline residues on protein conformation. J. Mol. Biol. 218, 397–412 (1991).
14 Shaw, A. C., van Balkom, I. D., Bauer, M., Cole, T. R., Delrue, M. A., Van Haeringen, A. et al. Phenotype and natural history in Marshall-Smith syndrome. Am. J. Med. Genet. A 152A, 2714–2726 (2010).
15 Cole, T. R. & Hughes, H. E. Sotos syndrome: a study of the diagnostic criteria and natural history. J. Med. Genet. 31, 20–32 (1994).

Supplementary Information accompanies the paper on Journal of Human Genetics website (http://www.nature.com/jhg)

ORIGINAL ARTICLE

A family of oculofaciocardiodental syndrome (OFCD) with a novel *BCOR* mutation and genomic rearrangements involving *NHS*

Yukiko Kondo[1], Hirotomo Saitsu[1], Toshinobu Miyamoto[2], Kiyomi Nishiyama[1], Yoshinori Tsurusaki[1], Hiroshi Doi[1], Noriko Miyake[1], Na-Kyung Ryoo[3], Jeong Hun Kim[3], Young Suk Yu[3] and Naomichi Matsumoto[1]

Oculofaciocardiodental syndrome (OFCD) is an X-linked dominant disorder associated with male lethality, presenting with congenital cataract, dysmorphic face, dental abnormalities and septal heart defects. Mutations in *BCOR* (encoding BCL-6-interacting corepressor) cause OFCD. Here, we report on a Korean family with common features of OFCD including bilateral 2nd–3rd toe syndactyly and septal heart defects in three affected females (mother and two daughters). Through the mutation screening and copy number analysis using genomic microarray, we identified a novel heterozygous mutation, c.888delG, in the *BCOR* gene and two interstitial microduplications at Xp22.2–22.13 and Xp21.3 in all the three affected females. The *BCOR* mutation may lead to a premature stop codon (p.N297IfsX80). The duplication at Xp22.2–22.13 involved the *NHS* gene causative for Nance–Horan syndrome, which is an X-linked disorder showing similar clinical features with OFCD in affected males, and in carrier females with milder presentation. Considering the presence of bilateral 2nd–3rd toe syndactyly and septal heart defects, which is unique to OFCD, the mutation in *BCOR* is likely to be the major determinant for the phenotypes in this family.
Journal of Human Genetics advance online publication, 2 February 2012; doi:10.1038/jhg.2012.4

INTRODUCTION

Oculofaciocardiodental syndrome (OFCD, Mendelian Inheritance in Man (MIM) #300166), an X-linked dominant disorder, is characterized by ocular, facial, cardiac and dental abnormalities associated with male lethality.[1,2] Mutations in the BCL-6 corepressor gene (*BCOR*, MIM *300485) at Xp11.4 cause OFCD.[3] *BCOR/Bcor* is ubiquitously expressed in human tissues and is strongly and specifically expressed in the eye, brain, neural tube and branchial arches during mouse embryonic development, which are affected in OFCD.[4,5] In 2009, Hilton *et al.*[6] clinically reviewed 35 cases with *BCOR* mutations and summarized the frequency of phenotypes: congenital cataract (100%), microphthalmia and/or microcornea (82%), facial dysmorphism (96%) including long narrow face and high nasal bridge, cardiac anomalies (74%, commonly septal defects), dental abnormalities (100%) such as delayed and/or primary dentition, root radiculomegaly, and absent/duplicated/fused teeth and mental retardation (18%).[6] Additionally, skeletal abnormalities such as 2nd–3rd toe syndactyly, hammer toes, and radioulnar synostosis are also observed in 97% patients. Various types of mutations in *BCOR* have been described including nonsense, small insertions or deletions and splice

site mutations, suggesting that the loss of functions (null allele) might result in OFCD. In addition, microdeletions involving *BCOR* have been also reported in individuals with OFCD. Most mutations predicted to generate premature stop codons, likely suffering from nonsense-mediated mRNA decay, although nonsense-mediated mRNA decay was unable to be confirmed because of the severe skewed X-inactivation in blood leukocytes.[3,6]

Nance–Horan syndrome (NHS) is an X-linked cataract-dental syndrome (MIM #302350) characterized by congenital cataract, dental abnormalities, facial dysmorphism and mental retardation.[7] Congenital cataract in affected male usually requires early surgery.[8] Dental abnormalities include maxillary and mandibular diastema of both central and lateral incisors, and screwdriver-shaped teeth because of narrow gingival and incisal margins.[9] Carrier females typically display posterior Y-sutural lens opacities, and the dental and facial anomalies of the syndrome may be observed, but with a milder presentation.[8] Mutations in *NHS* (MIM *300457) at Xp21.1-p22.3 cause NHS.[9–11] The most pathogenic mutations are truncating mutations. Coccia *et al.*[8] reported complex duplication-triplication rearrangements of the *NHS* gene in a family with congenital cataract and congenital

[1]Department of Human Genetics, Yokohama City University Graduate School of Medicine, Yokohama, Japan; [2]Department of Obstetrics and Gynecology, Asahikawa Medical College, Asahikawa, Japan and [3]Department of Ophthalmology, Seoul National University College of Medicine, Seoul, Korea
Correspondence: Dr N Matsumoto, Department of Human Genetics, Yokohama City University Graduate School of Medicine, Fukuura 3-9, Kanazawa-ku, Yokohama 236-0004, Japan.
E-mail: naomat@yokohama-cu.ac.jp
Received 3 October 2011; revised 6 December 2011; accepted 5 January 2012

heart defects in affected males, suggesting that genomic rearrangements of *NHS* are able to cause the X-linked cataract.

In this report, mutation screening and genomic microarray revealed a heterozygous mutation in *BCOR* and genomic rearrangements involving *NHS* in the three affected females of a Korean family with congenital cataract, dental abnormalities and 2nd–3rd toe syndactyly. Detailed molecular analysis will be presented.

MATERIALS AND METHODS

Clinical report

The Korean family with congenital cataract was previously described (as family 4) (Figure 1a).[12] Clinical features are summarized in Table 1. In the elder sister (MC17, the proband), bilateral congenital cataracts were noted 100 days after birth. Bilateral lensectomy and secondary intraocular lens insertion were performed. Ventricular septal defect, atrial septal defect, patent ductus arteriosus, delayed dentition, bilateral broad halluces, bilateral 2nd–3rd toe syndactyly, bilateral hammer toes and right brachyphalangia of fourth toe were also recognized. Mental development was normal. In the younger sister (MC18), bilateral congenital cataracts were also recognized. Bilateral lensectomy and secondary intraocular lens insertion were performed at ages of 2 months and 3 years, respectively. Right inguinal hernia, delayed dentition, and bilateral broad halluces, bilateral 2nd–3rd toe syndactyly, and bilateral hammer toes were noted (Figures 1b and c). She had learning difficulties at school, but IQ was not measured. In the mother (MC17b), bilateral congenital cataracts were noted and left lensectomy was performed at age of 10 years. Because of her dental anomalies and hypodontia, all her teeth were surgically removed. Bilateral 2nd–3rd toe syndactyly and bilateral hammer toes were noted. Her intelligence was normal. All the three affected members shared bilateral congenital cataracts, delayed dentition, bilateral 2nd–3rd toe syndactyly and bilateral hammer toes. Dysmorphic facial features were unseen.

DNA sequencing

Experimental protocols were approved by Institutional Review Boards for Ethical Issues at Yokohama City University School of Medicine and the Committee for the Ethical Issues on Human Genome and Gene Analysis, Seoul National University. Informed consent was obtained from all individuals. Genomic DNA was obtained from peripheral leukocytes using QIAGEN Blood and Cell Culture DNA Midi Kit (QIAGEN, Hilden, Germany). DNA was amplified using GenomiPhi V2 kit (GE healthcare, Buckinghamshire, UK). In *BCOR*, there are three isoforms: isoform a (GenBank accession number NM_017745.5), isoform b (GenBank accession number NM_001123384.1) and isoform c (GenBank accession number NM_001123385.1). In *NHS*, there are two isoforms: isoform 1 (GenBank accession number NM_198270.2) and isoform 2 (GenBank accession number NM_001136024.2). Nucleotide sequences of 1st to 15th exons of *BCOR* and 1st to 8th exons of *NHS* covering all the protein coding region as well as exon–intron borders were analyzed. Polymerase chain reaction (PCR) conditions and primer information are shown in Supplementary Table 1. PCR products were purified with ExoSAP (USB, Cleveland, OH, USA) and sequenced with BigDye terminator 3.1 (Applied Biosystems, Foster City, CA, USA) on 3100 and 3500×1 Genetic Analyzer (Applied Biosystems). Sequences of patients were compared with the reference human genome sequences (based on the UCSC Genome Browser coordinate, February 2009) with Sequencher 4.10.1. (Gene Codes, Ann Arbor, MI, USA).

Copy number analysis

Copy number variations (CNVs) were investigated by Cytogenetics Whole-Genome 2.7 M. Array (Affymetrix, Santa Clara, CA, USA) based on the manufacturer's instruction using 100 ng genomic DNA from three affected females (MC17b, MC17 and MC18). Copy number alterations were analyzed by Chromosome Analysis Suite (Affymetrix) with NetAffx 30.1 annotations (hg18 assembly). Any filters such as minimum size and probe numbers of CNVs were not applied. The selection criteria for putative pathogenic CNVs were as follows: (1) CNVs were shared with three affected females, (2) CNVs
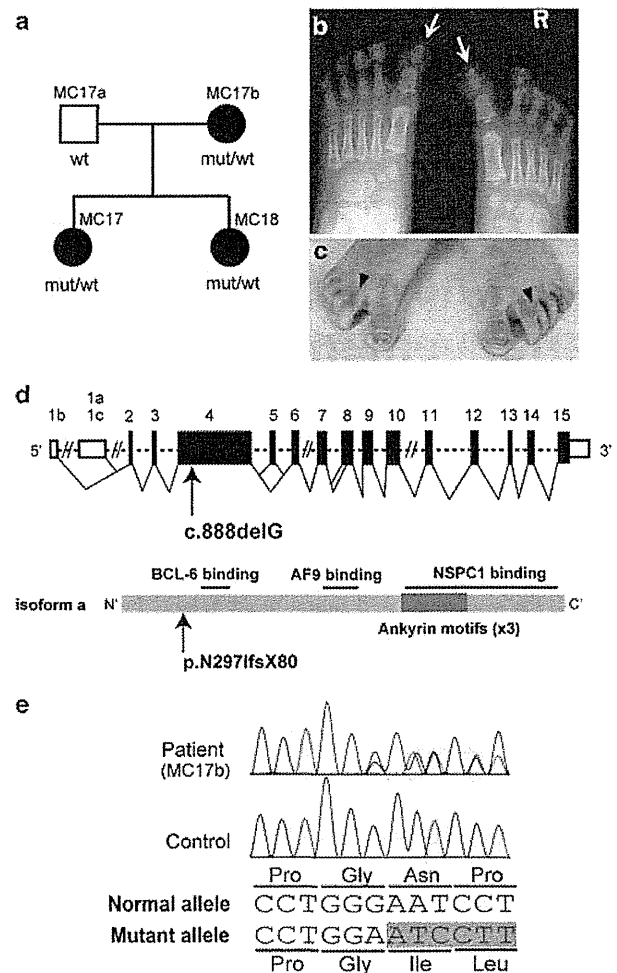

Figure 1 Pedigree, foot malformation and a *BCOR* mutation found in the family. (a) Familial pedigree. Black and open symbols denote affected and unaffected individuals, respectively. (b, c) Bilateral broad halluces (the big toe, arrows in b), bilateral 2nd–3rd cutaneous syndactyly (arrowheads in c) and bilateral hammer toes in MC18. (d) Schematic representation of the *BCOR* gene (top). UTR and coding region are open and filled rectangles, respectively. Alternative splicing by three different isoforms is shown. The isoform b is absence of exon 5 and the isoform c is 102bp and 156bp longer than the isoform a and b, respectively. The location of the c.888delG mutation is indicated by an arrow. The protein structure of BCOR (isoform a, bottom). Three consecutive ankyrin motifs are indicated as a dark-gray box. The three binding sites for BCL-6, AF9 and NSPC1 are indicated with horizontal bars. (e) Electropherograms showing the mutation in the affected patient (MC17b) (top) and a control (bottom). A single nucleotide deletion in exon 4 results in a frameshift. mut, a mutant allele; wt, a wild type allele.

encompassed exons and (3) CNVs were not present in the Database of Genomic Variants (http://projects.tcag.ca/variation/).

Cloning of duplication breakpoints

DNA of the affected mother (MC17b) was digested with restriction enzymes: *Eco*RI, *Nsi*I, *Xba*I, *Bam*HI and *Bgl*II (New England Biolabs, Beverly, MA, USA). Digested DNA was self-ligated by Ligation High ver. 2 (Toyobo, Osaka, Japan), precipitated with ethanol, and dissolved in 20 µl EB buffer (QIAGEN, Tokyo, Japan). Inverse PCR was performed in 25 µl volume containing 2 µl ligated DNA, 1× PCR buffer for KOD FX, 0.4 mM each dNTPs, 0.5 µM each primer and

Table 1 Clinical features of patients with a *BCOR* mutation

	MC17b	MC17	MC18
Age	41	11	8
Sex	Female	Female	Female
Ocular features			
Congenital cataract	+	+	+
Microphthalmia/microcornea	–	–	–
Coloboma	–	–	–
Ptosis	–	–	–
Secondary glaucoma	–	+	+
Nystagmus	–	–	–
Cardiac features	–	+	–
Septal defects	–	+	–
Patent ductus arteriosus	–	+	–
Dental features			
Delayed/persistent/unerupted dentition	+	+	+
Root radiculomegaly (secondary teeth)	ND	ND	ND
Hypodontia (secondary teeth)	+	ND	ND
Duplication/fusion (secondary teeth)	ND	ND	ND
Skeletal features			
Hammer toes (camptodactyly)	+	+	+
Second–third toe syndactyly	+	+	+
Broad halluces (big toe)	–	+	+
Brachyphalangia of the fourth right toe	–	+	–
Radioulnar synostosis	ND	ND	ND
Lodosis/scoliosis/vertebral fusion	ND	ND	ND
Other features			
Mental retardation	–	–	+
Hearing impairment	–	ND	ND
Inguinal hernia	–	–	+

Abbreviation: ND, Not determined.
A plus (+) or minus (–) sign denotes the presence or absence of a particular physical feature.

0.5 U KOD FX polymerase (Toyobo). PCR were cycled 35 times at 98 °C for 10 s, 68 °C for 10 min. PCR products electrophoresed in 1% agarose gel were stained with ethidium bromide and the aberrant band was extracted using QIAEXII Gel Extraction Kit (QIAGEN, Tokyo, Japan) and sequenced. Primer information is available on request.

X inactivation study and haplotype analysis

X inactivation pattern was studied using the human androgen receptor assay and fragile X mental retardation locus methylation assay as previously described.[13–15] Briefly, genomic DNA of a patient (MC17), the parents (MC17a and MC17b), a control male and a control female was digested with two methylation-sensitive enzymes, HpaII and HhaI. PCR was performed with human androgen receptor assay primers (FAM-labeled ARf: 5′-CCAGAAT CTGTTCCAGAGCGTGC-3′; ARr: 5′-CTCTACGATGGGCTTGGGGAGAA C-3′)[16] and fragile X mental retardation assay primers (FAM-labeled FMR1f: 5′-AGCCCCGCACTTCCACCACCAGCTCCTCCA-3′; FMR1r: 5′-GCTCAGCT CCGTTTCGGTTTCACTTCCGGT-3′). Fluorescent-labeled products were analyzed on an ABI PRISM 3100 or 3130×1 Genetic analyzer and GeneMapper Software version 4.0 (Applied Biosystems). One of affected females (MC18) was not analyzed because of insufficient amount of genomic DNA. According to published criteria, X inactivation ratios of ≤80:20 were considered random and ratios >80:20 were considered skewed and ratios >90:10 were considered highly skewed.[16,17]

X chromosome haplotype was analyzed using 12 microsatellite markers (*DXS1060, DXS8051, DXS987, DXS1226, DXS1214, DXS1068, DXS993, DXS991, DXS986, DXS8055, DXS1047* and *DXS1073*). Fluorescent- labeled (either FAM, VIC or NED) forward primers and tailed reverse primers were purchased from Applied Biosystems. These markers were based on the Marshfield genetic map (http://research.marshfieldclinic.org/genetics). PCR was cycled 40 times at 94 °C for 30 s, 55 °C for 30 s and 72 °C for 30 s in 10 µl volume containing 50 ng DNA, 1× ExTaq buffer, 0.2 mM each dNTP, 0.4 µM each primer and 0.1 U ExTaq HS polymerase. Haplotypes were manually constructed.

RESULTS

We detected a *BCOR* mutation, c. 888delG in MC17, MC17b and MC18 (Figures 1d and e). The mutation may result in insertion of 80 new amino acids after the mutation site with a premature stop codon at position 377 (p.N297IfsX80). The mutation was completely co-segregated with OFCD phenotypes in this family (Figure 1a). Sequencing of the entire *NHS* coding region detected no pathological mutations in this family.

The Cytogenetics Whole-Genome 2.7 M array detected a total of 48 CNVs (12 duplications and 36 deletions) in any of the affected females. The CNVs, which encompassed exons, were 8 duplications and 13 deletions. Among them, two duplications and one deletion were shared with three affected females. The one deletion was present in the Database of Genomic Variants. Thus, the CNVs fulfilling the criteria for pathogenic CNVs were two interstitial duplications. The 740-kb duplication at Xp22.2–22.13 encompassed exons 2–18 of *REPS2* (MIM *300317) and exons 1–3 of *NHS*. The other 110-kb duplication at Xp21.3 contained exon 2 of interleukin-1 receptor accessory protein-like 1 (*IL1RAPL1*) (MIM *300206) (Figure 2a). We were unable to examine the duplications by fluorescent *in situ* hybridization because only DNA samples were available. Instead, inverse PCR of self-ligated DNA with different sets of primers was able to amplify an expected fragment from normal *NHS* allele in all sets of primers, suggesting that the presence of one or more normal *NHS* alleles (Figures 2b and c). In addition, several attempts successfully cloned one of rearrangement junctions in relation to *NHS* (Figure 2c). This aberrant band showed that the sequences of intron 1 of *IL1RAPL1* followed the sequences of intron 3 of *NHS*, suggesting that two duplications were tandemly connected (Figure 2d, upper cases). More complicatedly, 62-bp sequences of intron 3 of *IL1RAPL1* with inverted orientation were inserted between intron 3 of *NHS* and intron 1 of *IL1RAPL1* (Figure 2d, lower cases). The other possible breakpoints, which may result in disruption of *NHS* locus could not be determined regardless of rigorous attempts. Thus there seems to be two normal *NHS* alleles and an extra *NHS* allele, in which exons 1–3 of *NHS* was connected to exon 2 of *IL1RAPL1*. Copy number of the *BCOR* gene was normal. In human androgen receptor assays, the mother (MC17b) was skewed pattern (8%), whereas the elder sister (MC17) showed a random pattern (26%). In fragile X mental retardation assays, the mother (MC17b) and elder sister (MC17) showed a highly skewed pattern (<1%) and a random pattern (48%), respectively. X-chromosome haplotype analysis was able to separate all the alleles in this family (Supplementary Figure 1). The inactivated allele in the mother harbored the *BCOR* mutation and the *NHS* rearrangement.

DISCUSSION

BCOR functions as a corepressor of BCL-6, which is a POZ/zinc finger transcription repressor.[4] BCOR have three consecutive ankyrin motifs, an AF9 (ALL1 fused gene from chromosome 9) binding site and an NSPC1 (nervous system polycomb-1) binding site.[4,18,19] Recently, the
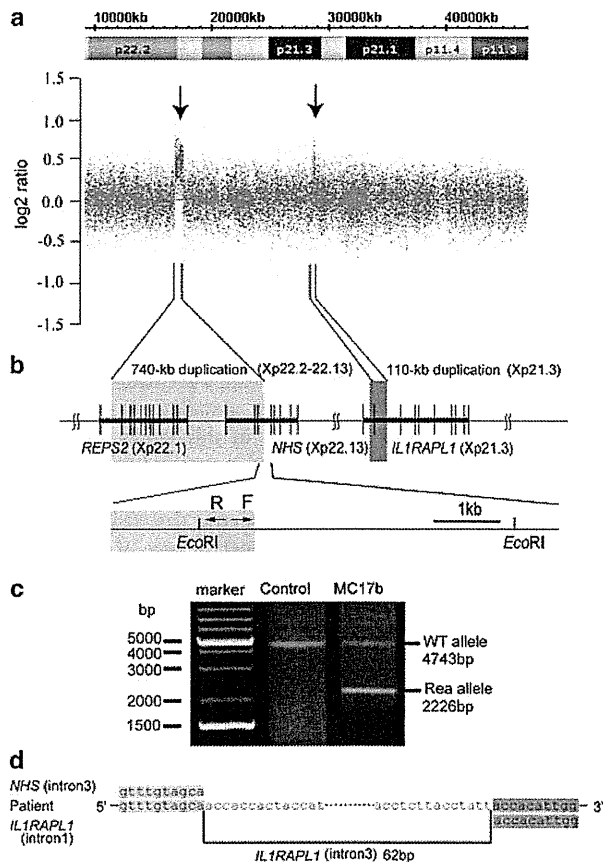
Figure 2 Two microduplications at Xp22.2–22.13 and Xp21.3. (a) Array profile of a part of chromosome X in the elder sister (MC17). x and y axis show the genomic location from the p telomere of chromosome X (UCSC coordinates, May, 2006) (upper) and $\log_2$ (Signal ratio) values (lower), respectively. The 740-kb duplication at Xp22.2–22.13 and the 110-kb duplication at Xp21.3 are indicated by arrows. (b) Upper shows schematic representation of two duplicated regions (highlighted in gray). Three genes (REPS2, NHS and IL1RAPL1) are oriented in the same direction (from centromere to telomere). Lower indicates scheme of inverse PCR using self-ligated DNA after digestion with EcoRI. Primers are shown by arrows (F, forward; R, reverse). (c) Gel image of inverse PCR products performed as shown in (b). Upper and lower bands represent wild-type allele (WT allele) and rearranged allele (Rea allele), respectively. The DNA of both bands was extracted from agarose gel and sequenced. (d) Sequence of a Rea allele is shown. The top, middle and bottom indicate sequences of the intron 3 of NHS, rearranged junction and intron 1 of IL1RAPL1, respectively. The 62 nucleotides of intron 3 of IL1RAPL1 (lower cases) were inserted in an inverted orientation between intron 3 of NHS and intron 1 of IL1RAPL1. Matched sequences are highlighted with gray shadows.

minimal BCL-6 binding site was identified within residues 498–514, which is located in exon 4.[20] In this study, a novel BCOR mutation, c.888delG (p.N297IfsX80) in exon 4, was found in this family. We assumed the mutant transcript with this mutation may undergo nonsense-mediated mRNA decay, but we could not confirm it as no living cells were available from the patients. A total of 31 mutations in BCOR were registered in Human Gene Mutation Database (http://www.biobase-international.com/). All the mutations result in premature stop codons. Exon 4 harbors 40% of mutations (12/30), leading to truncated proteins lacking BCL-6, AF9 and NSPC1 binding sites, and ankyrin motifs if translated. Lack of BCL-6 binding site could not

explain the OFCD phenotypes because BCL-6-deficient mice did not show ocular, dental and skeletal phenotypes.[21,22] Moreover, an OFCD mutant protein, that lacked ankyrin motifs and NSPC1 binding site, showed transcriptional repression activity similar to that of wild type.[3] Thus, the c.888delG mutation in BCOR may be associated with loss of BCOR transcripts through nonsense-mediated mRNA decay.

By genomic microarray, two microduplications were detected in MC17, MC18 and MC17b: one at Xp22.2–22.13 involving a part of REPS2 and NHS, and the other at Xp21.3 containing exon 2 of IL1RAPL1. Previously, complex duplication-triplication rearrangements of the NHS gene in a family with congenital cataract were reported, suggesting that genomic rearrangements of NHS are able to cause the X-linked cataract.[8] This family did not show the typical features of NHS such as dental anomalies, dysmorphism and developmental delay, and congenital heart defects were diagnosed in four out of six affected males. The complex rearrangement consists of triplication embedded within a duplication region. The triplicated region includes the NHS genes except exon 1, and the entire SCML1 and RAI2 genes. Coccia et al.[8] described that the additional phenotype of congenital heart defects observed in some affected males could be because of perturbed NHS gene transcription or increased dosage of the NHS, SCML1 or RAI2 genes. In our cases, two normal NHS alleles may exist in addition to an extra NHS allele, in which exons 1–3 of NHS was connected to individual exon 2 of IL1RAPL1, keeping the protein coding frame if properly spliced. Because the transcript from the extra NHS allele did not have polyA signal sequences, the allele is likely to produce no functional protein. Thus, the situation was totally different between our cases and Coccia's et al.'s[8] cases.

Recently, Honda et al.[23] reported two unrelated X-linked mental retardation Japanese families, which possessed the similar duplication found in our Korean family: the 737-kb duplication at Xp22.2, which contains a part of REPS2 and NHS, and the 100-kb duplication at Xp21.3, which contains a part of IL1RAPL1. In their report, fluorescent in situ hybridization analysis revealed that the clone RP11-438J7, which entirely covered the duplication at Xp21.3, demonstrated two distinct signals at Xp in metaphases, suggesting that the duplication at Xp21.3 was inserted separately from the original site. The clone RP11-2K15 at Xp22.2, spanning the breakpoint of REPS2, showed one bright strong signal, suggesting that the duplication at Xp22.2 occurred in the proximity. Interestingly, the one of two signals of the RP11-438J7 was close to that of RP11-2K15 at Xp22.2, suggesting that the duplication involving IL1RAPL1 was inserted at Xp22.2. Their result is consistent with our data of the duplication breakpoint, in which the breakpoint in NHS was connected with the breakpoint of IL1RAPL1. Based on our experiences, high-density array experiments of >500 Japanese cases never showed such the genomic rearrangement involving NHS, implying that the rearrangement is very rare in Japanese population. It is noteworthy that congenital cataract and dental abnormalities were not pointed out in all the members (males and carrier females).[23] Thus, it is unlikely that the genomic rearrangement involving NHS causes congenital cataract and dental abnormalities as found in our family.

IL1RAPL1 is a causative gene for X-linked mental retardation,[24] and the microduplication at Xp21.3 containing exon 2 of IL1RAPL1 was suggested to cause MR in affected males.[23] Most carrier females of IL1RAPL1 mutations and the carrier mother of the microduplication involving IL1RAPL1 showed normal intelligence.[23–25] In this study, one of the three affected females (MC18) had learning difficulties at school, which could be mild presentation of MR. As 18% of patients with BCOR mutations showed MR,[6] it is reasonable that the BCOR mutation, rather than IL1RAPL1 rearrangement, causes mild MR in MC18.

Skewed and random X-inactivation in the mother (MC17b) and the elder daughter (MC17) was confirmed, respectively, in this family. In OFCD, skewed X-inactivation with the preferential inactivation of the mutated allele were recognized in eight affected females (like the mother, MC17b), suggesting that the *BCOR* mutations may lead to a selective disadvantage in blood leukocytes.[3,26] However, it has been reported that the X-inactivation pattern in blood leukocytes are unable to determine the severity of disease phenotypes as X-inactivation pattern may vary among tissues.[27] We suspect that X-inactivation pattern is different between peripheral blood leukocytes and respective tissues associated with OFCD phenotype.

In conclusion, a new OFCD family is described with a novel *BCOR* mutation. Clinical features overlap between OFCD and NHS, both of which belong to a spectrum of X-linked microphthalmia disorders.[6] Our cases have a *BCOR* mutation and genomic rearrangements involving *NHS*, confusing us to address the genetic etiology in the family. However, the presence of bilateral 2nd–3rd toe syndactyly and septal heart defects, which is unique to OFCD, can lead us to the conclusion that the *BCOR* mutation is the major determinant for the phenotypes in this family. Careful examination of associated anomalies will be useful for genetic testing of X-linked microphthalmia disorders.

ACKNOWLEDGEMENTS

Web Resources

The URLs for data presented herein are as follows: UCSC Genome Browser, http://genome.ucsc.edu/cgi-bin/hgGateway

1 Wilkie, A. O., Taylor, D., Scambler, P. J. & Baraitser, M. Congenital cataract, microphthalmia and septal heart defect in two generations: a new syndrome? *Clin. Dysmorphol.* **2**, 114–119 (1993).

2 Aalfs, C. M., Oosterwijk, J. C., van Schooneveld, M. J., Begeman, C. J., Wabeke, K. B. & Hennekam, R. C. Cataracts, radiculomegaly, septal heart defects and hearing loss in two unrelated adult females with normal intelligence and similar facial appearance: confirmation of a syndrome? *Clin. Dysmorphol.* **5**, 93–103 (1996).

3 Ng, D., Thakker, N., Corcoran, C. M., Donnai, D., Perveen, R., Schneider, A. *et al.* Oculofaciocardiodental and Lenz microphthalmia syndromes result from distinct classes of mutations in *BCOR. Nat. Genet.* **36**, 411–416 (2004).

4 Huynh, K. D., Fischle, W., Verdin, E. & Bardwell, V. J. BCoR, a novel corepressor involved in BCL-6 repression. *Genes Dev.* **14**, 1810–1823 (2000).

5 Wamstad, J. A. & Bardwell, V. J. Characterization of *Bcor* expression in mouse development. *Gene Expr. Patterns* **7**, 550–557 (2007).

6 Hilton, E., Johnston, J., Whalen, S., Okamoto, N., Hatsukawa, Y., Nishio, J. *et al. BCOR* analysis in patients with OFCD and Lenz microphthalmia syndromes, mental retardation with ocular anomalies, and cardiac laterality defects. *Eur. J. Hum. Genet.* **17**, 1325–1335 (2009).

7 Nance, W. E., Warburg, M., Bixler, D. & Helveston, E. M. Congenital X-linked cataract, dental anomalies and brachymetacarpalia. *Birth Defects Orig. Artic. Ser.* **10**, 285–291 (1974).

8 Coccia, M., Brooks, S. P., Webb, T. R., Christodoulou, K., Wozniak, I. O., Murday, V. *et al.* X-linked cataract and Nance-Horan syndrome are allelic disorders. *Hum. Mol. Genet.* **18**, 2643–2655 (2009).

9 Lewis, R. A., Nussbaum, R. L. & Stambolian, D. Mapping X-linked ophthalmic diseases. IV. Provisional assignment of the locus for X-linked congenital cataracts and micro-cornea (the Nance-Horan syndrome) to Xp22.2-p22.3. *Ophthalmology.* **97**, 110–120; discussion 120–111 (1990).

10 Stambolian, D., Lewis, R. A., Buetow, K., Bond, A. & Nussbaum, R. Nance-Horan syndrome: localization within the region Xp21.1-Xp22.3 by linkage analysis. *Am. J. Hum. Genet.* **47**, 13–19 (1990).

11 Burdon, K. P., McKay, J. D., Sale, M. M., Russell-Eggitt, I. M., Mackey, D. A., Wirth, M. G. *et al.* Mutations in a novel gene, *NHS*, cause the pleiotropic effects of Nance-Horan syndrome, including severe congenital cataract, dental anomalies, and mental retardation. *Am. J. Hum. Genet.* **73**, 1120–1130 (2003).

12 Miyamoto, T., Yu, Y. S., Sato, H., Hayashi, H., Sakugawa, N., Ishikawa, M. *et al.* Mutational analysis of the human *MBX* gene in four Korean families demonstrating microphthalmia with congenital cataract. *Turk J. Pediatr.* **49**, 334–336 (2007).

13 Allen, R. C., Zoghbi, H. Y., Moseley, A. B., Rosenblatt, H. M. & Belmont, J. W. Methylation of *Hpa*II and *Hha*I sites near the polymorphic CAG repeat in the human androgen-receptor gene correlates with X chromosome inactivation. *Am. J. Hum. Genet.* **51**, 1229–1239 (1992).

14 Carrel, L. & Willard, H. F. An assay for X inactivation based on differential methylation at the fragile X locus, *FMR1. Am. J. Med. Genet.* **64**, 27–30 (1996).

15 Nishimura-Tadaki, A., Wada, T., Bano, G., Gough, K., Warner, J., Kosho, T. *et al.* Breakpoint determination of X; autosome balanced translocations in four patients with premature ovarian failure. *J. Hum. Genet.* **56**, 156–160 (2011).

16 Kubota, T., Nonoyama, S., Tonoki, H., Masuno, M., Imaizumi, K., Kojima, M. *et al.* A new assay for the analysis of X-chromosome inactivation based on methylation-specific PCR. *Hum. Genet.* **104**, 49–55 (1999).

17 Amos-Landgraf, J. M., Cottle, A., Plenge, R. M., Friez, M., Schwartz, C. E., Longshore, J. *et al.* X chromosome-inactivation patterns of 1,005 phenotypically unaffected females. *Am. J. Hum. Genet.* **79**, 493–499 (2006).

18 Srinivasan, R. S., de Erkenez, A. C. & Hemenway, C. S. The mixed lineage leukemia fusion partner AF9 binds specific isoforms of the BCL-6 corepressor. *Oncogene* **22**, 3395–3406 (2003).

19 Gearhart, M. D., Corcoran, C. M., Wamstad, J. A. & Bardwell, V. J. Polycomb group and SCF ubiquitin ligases are found in a novel BCOR complex that is recruited to BCL6 targets. *Mol. Cell Biol.* **26**, 6880–6889 (2006).

20 Ghetu, A. F., Corcoran, C. M., Cerchietti, L., Bardwell, V. J., Melnick, A. & Prive, G. G. Structure of a BCOR corepressor peptide in complex with the BCL6 BTB domain dimer. *Mol. Cell.* **29**, 384–391 (2008).

21 Ye, B. H., Cattoretti, G., Shen, Q., Zhang, J., Hawe, N., de Waard, R. *et al.* The *BCL-6* proto-oncogene controls germinal-centre formation and Th2-type inflammation. *Nat. Genet.* **16**, 161–170 (1997).

22 Dent, A. L., Shaffer, A. L., Yu, X., Allman, D. & Staudt, L. M. Control of inflammation, cytokine expression, and germinal center formation by BCL-6. *Science* **276**, 589–592 (1997).

23 Honda, S., Hayashi, S., Imoto, I., Toyama, J., Okazawa, H., Nakagawa, E. *et al.* Copy-number variations on the X chromosome in Japanese patients with mental retardation detected by array-based comparative genomic hybridization analysis. *J. Hum. Genet.* **55**, 590–599 (2010).

24 Carrie, A., Jun, L., Bienvenu, T., Vinet, M. C., McDonell, N., Couvert, P. *et al.* A new member of the IL-1 receptor family highly expressed in hippocampus and involved in X-linked mental retardation. *Nat. Genet.* **23**, 25–31 (1999).

25 Nawara, M., Klapecki, J., Borg, K., Jurek, M., Moreno, S., Tryfon, J. *et al.* Novel mutation of *IL1RAPL1* gene in a nonspecific X-linked mental retardation (MRX) family. *Am. J. Med. Genet. A* **146A**, 3167–3172 (2008).

26 Hedera, P. & Gorski, J. L. Oculo-facio-cardio-dental syndrome: skewed X chromosome inactivation in mother and daughter suggest X-linked dominant inheritance. *Am. J. Med. Genet. A* **123A**, 261–266 (2003).

27 Bartnik, M., Derwinska, K., Gos, M., Obersztyn, E., Kolodziejska, K. E., Erez, A. *et al.* Early-onset seizures due to mosaic exonic deletions of *CDKL5* in a male and two females. *Genet. Med.* **13**, 447–452 (2011).

Supplementary Information accompanies the paper on Journal of Human Genetics website (http://www.nature.com/jhg)

SHORT REPORT

Identification of a novel in-frame *de novo* mutation in *SPTAN1* in intellectual disability and pontocerebellar atrophy

Fadi F Hamdan[1,6], Hirotomo Saitsu[2,6], Kiyomi Nishiyama[2], Julie Gauthier[3], Sylvia Dobrzeniecka[3], Dan Spiegelman[3], Jean-Claude Lacaille[4], Jean-Claude Décarie[5], Naomichi Matsumoto[2], Guy A Rouleau[3] and Jacques L Michaud[*,1]

Heterozygous in-frame mutations (p.E2207del and p.R2308_M2309dup) in the α-II subunit of spectrin (SPTAN1) were recently identified in two patients with intellectual disability (ID), infantile spasms (IS), hypomyelination, and brain atrophy. These mutations affected the C-terminal domain of the protein, which contains the nucleation site of the α/β spectrin heterodimer. By screening *SPTAN1* in 95 patients with idiopathic ID, we found a *de novo* in-frame mutation (p.Q2202del) in the same C-terminal domain in a patient with mild generalized epilepsy and pontocerebellar atrophy, but without IS, hypomyelination, or other brain structural defects, allowing us to define the core phenotype associated with these C-terminal SPTAN1 mutations. We also found a *de novo* missense variant (p.R566P) of unclear clinical significance in a patient with non-syndromic ID. These two mutations induced different patterns of aggregation between spectrin subunits in transfected neuronal cell lines, providing a paradigm for the classification of candidate variants.
European Journal of Human Genetics advance online publication, 18 January 2012; doi:10.1038/ejhg.2011.271

INTRODUCTION

The targeting and maintenance of groups of proteins at specific membrane domains of neurons, such as the synapse and the axon, are critical for the brain function and development. Not surprisingly, mutations in proteins that participate in the assembling of these domains, such as the spectrins, have been shown to cause neurological disorders. Spectrins consist of α- and β-subunits that form antiparallel heterodimers, which are assembled to form heterotetramers in a head-to-head configuration.[1,2] Heterozygous mutations in the β-III subunit (SPTBN2) were shown to cause spinocerebellar ataxia type-5.[3] Recently, *de novo* in-frame mutations in the α-II spectrin subunit (SPTAN1) were identified in patients with severe intellectual disability (ID), infantile spasms (IS) with hypsarrhythmia, hypomyelination, and atrophy of various regions of the brain, including the cerebellum and brainstem.[4] These mutations are located in a C-terminal domain that includes the nucleation site involved in α/β spectrin heterodimer formation.[5] Biochemical studies indicated that these mutations destabilized this interaction, leading to aggregation of α-II(mut)/β-II and α-II(mut)/β-III spectrin heterodimers in mouse cortical neurons and in lymphoblastoid cells from the patients.[4]

Recent studies suggest that *de novo* point mutations in the germ line, which in humans are estimated to occur at a rate of $\sim 1.1 \times 10^{-8}$ per base, may explain a large fraction of ID cases.[6–8] In the course of a project aimed to identify such mutations in candidate synaptic genes,

we sequenced *SPTAN1* in patients with idiopathic ID. We identified *de novo* mutations in *SPTAN1* in a patient with non-syndromic ID and in a patient with ID, epilepsy and pontocerebellar atrophy, further expanding the phenotypical spectrum associated with mutations in *SPTAN1*. Moreover, we found that these mutations induce different patterns of aggregations of spectrin subunits in cultured neuronal cells, providing a paradigm to validate candidate variants and to establish correlations between genotypes and phenotypes.

METHODS

Subjects and DNA sequencing

Ninety-five cases of idiopathic ID (46 males and 49 females), mostly of French–Canadian ethnicity, without growth abnormalities or specific dysmorphic features, as well as 190 French–Canadians controls were studied. A subset of the ID cases (25/95) also displayed epilepsy. Genomic DNA was extracted from blood samples (Qiagen/Gentra, Toronto, ON, Canada) and paternity/maternity was confirmed using six informative unlinked microsatellite markers (Supplementary Table S1). Polymerase chain reaction amplification of all *SPTAN1*-coding exons and their splice junctions (Supplementary Table S2 for primers), DNA sequencing, and mutation analyses are detailed in the Supplementary Information.

Expression vectors

SPTAN1 mutants (c.1697G>C/p.R566P, c.6605_6607del/p.Q2202del, c.6619_6621del/p.E2207del; positions based on Refseq NM_001130438.2) were generated by site-directed mutagenesis using KOD-Plus-Mutagenesis kit

[1]Centre of Excellence in Neuroscience of Université de Montréal (CENUM), Centre de Recherche du CHU Sainte-Justine, Montréal, Quebec, Canada; [2]Department of Human Genetics, Yokohama City University Graduate School of Medicine, Yokohama, Japan; [3]Centre of Excellence in Neuroscience of Université de Montréal (CENUM) and Centre de Recherche du Centre Hospitalier de l'Université de Montréal (CRCHUM), and Department of Medicine, Université de Montréal, Montreal, Quebec, Canada; [4]Le Groupe de Recherche sur le Système Nerveux Central, Department of Physiology, Université de Montréal, Montréal, Quebec, Canada; [5]Department of Medical Imaging, CHU Sainte-Justine, Montréal, Quebec, Canada
*Correspondence: Dr JL Michaud, Centre of Excellence in Neuroscience of Université de Montréal (CENUM), Centre de Recherche du CHU Sainte-Justine, 3175 Côte Sainte-Catherine, Montreal, Quebec H3T 1C5, Canada. Tel: +1 514 345 4931, ext: 6900, Fax: +1 514 345 4766; E-mail: jacques.michaud@recherche-ste-justine.qc.ca
[6]These authors contributed equally to this work.
Received 20 July 2011; revised 30 November 2011; accepted 7 December 2011

(Toyobo, Osaka, Japan), and verified by sequencing. A full-length human *SPTAN1* cDNA (α-II spectrin) with a C-terminal Flag-tag was cloned into a CAG-promoter vector to express C'-Flag-tagged α-II spectrin.

Cell culture, transfection, and immunofluorescence

Mouse neuroblastoma 2A (N2A) cells and primary cultures of mouse cortical neurons were grown, transfected, and tested by immunofluorescence for the expression of wild type and mutant spectrin subunits, as previously described,[4,9] and detailed in the Supplementary Information.

RESULTS

We identified three heterozygous variants in *SPTAN1* in different patients, including two missense (c.1679A>G/p.E560G and c.1697G >C/p.R566P) and one in-frame amino-acid deletion (c.6605_6607del/p.Q2202del). p.E560G was transmitted from a healthy mother and is predicted not to affect protein function by various algorithms (Supplementary Table S3). In contrast, p.R566P (patient-1) and p.Q2202del (patient-2) were absent from the blood DNA of the corresponding healthy parents, indicating that they were

de novo, and were not detected in 190 French–Canadian controls, nor reported in dbSNP134. p.R566P affects a well-conserved residue that lies at the N-terminus of SPTAN1 and is predicted to damage protein function by SIFT[10] and polyphen.[11] The deleted p.Q2202 residue is part of a C-terminal domain required for α/β spectrin subunit heterodimer formation.[5] Interestingly, p.Q2202del is in close proximity to the recently reported *SPTAN1* in-frame mutations, p.E2207del and p.R2308_M2309dup, identified in patients with ID, IS, and structural brain defects (Figure 1).[4]

The phenotypes of the patients with p.R566P and p.E2207del were different (Supplementary Information). Patient-1 (p.R566P), a 9-year-old boy, shows mild non-syndromic ID without epilepsy. The brain CT-scan did not reveal any abnormality. He has a sister who also shows non-syndromic ID but who does not carry the mutation. Patient-2 (p.Q2202del), an 11-year-old boy, shows severe ID. He did not present with IS but developed mild generalized epilepsy. The brain MRI showed severe atrophy of the cerebellum and mild atrophy of the brainstem, without any hypomyelination or other structural defects (Figure 2).
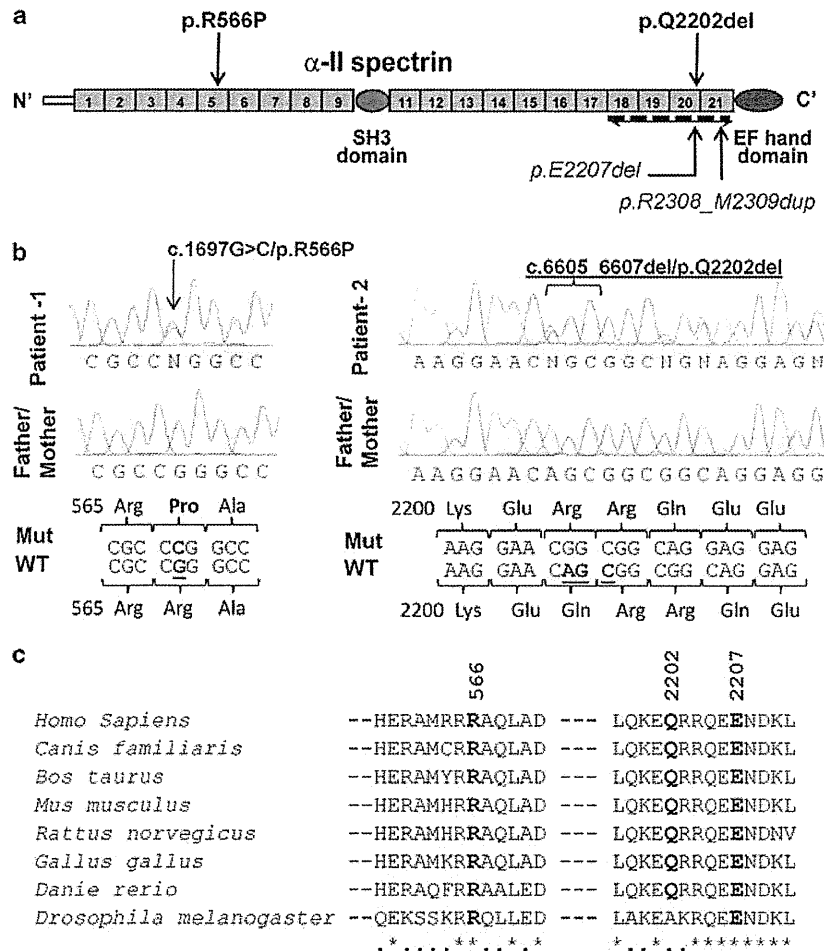

Figure 1 *De novo* mutations identified in *SPTAN1*. (a) Schematic representation of the SPTAN1 protein consisting of 22 domains, including 20-spectrin repeats, an SH3 domain, and an EF hand domains. The last four spectrin repeats required for α/β spectrin heterodimer associations are indicated (bidirectional arrow). Mutations identified in this study (p.R566P and p.Q2202del) and those by Saitsu *et al*[4] (p.E2207del and p.R2308_M2309dup) are shown. (b) Chromatograms of the *de novo* p.R566P and p.Q2202del mutations (Mut) and wildtype (WT) *SPTAN1* sequences. (c) Amino-acid conservation of the SPTAN1 residues affected with *de novo* mutations (p.R566P, p.Q2202del and p.E2207del). Amino-acid alignments were generated by homologene (NCBI) and the amino-acid sequences flanking the mutations are shown.
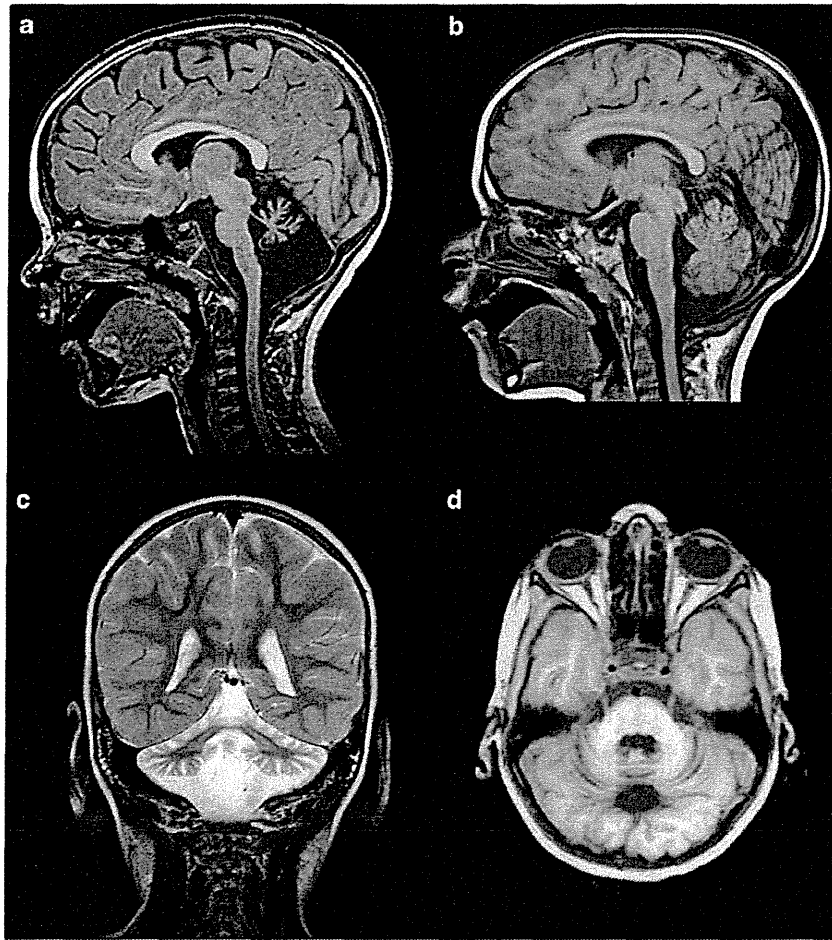
Figure 2 The brain MRI of the patient with p.Q2202del showing pontocerebellar atrophy. (a) Sagittal T1 image at midline showing severe atrophy of vermis with hypoplastic brainstem. The corpus callosum is larger than normal for the age of the patient. (b) Sagittal T1 image of an age and gender matched control showing normal pons and normal cerebellum (c) Coronal T2 image of the patient at the level of the posterior fossa, showing severe atrophy of both cerebellar hemispheres with T2 hypersignal of both middle cerebellar pedoncule. (d) Axial T1 image of the patient at the level of the cerebellum showing diffuse cerebellar atrophy.

Expression of α-II spectrin containing p.E2207del or p.R2308_M2309dup induced subunit aggregates in primary neuronal cultures.[4] We took advantage of this assay to compare the impact of p.R566P, p.Q2202del, and p.E2207del in mouse N2A cells and mouse cortical neurons (Figure 3). Expression of wild-type α-II spectrin in N2A cells resulted in its localization at cell periphery, without the formation of aggregates (Figures 3a and b). The p.Q2202del mutant showed a similar pattern of expression whereas the p.E2207del induced small aggregates in 6% of transfected cells. In contrast, the p.R566P mutant induced large aggregates in 86% of transfected N2A cells. These mutant α-II spectrin aggregates colocalized with endogenous β-II spectrin (Supplementary Figure S1). No endogenous β-III-spectrin subunits were detectable in N2A cells by immunofluorescence. In primary neuronal cultures, p.E2207del induced aggregates in most cells; these aggregates were composed of both β-II and β-III spectrin subunits (Figures 3b-d). The p.Q2202del mutant showed a similar aggregation profile, but in a lower proportion of cells (15–20%). In contrast, p.R566P induced aggregates in a much smaller number of cells (<5%). Moreover, double immunostaining revealed that these aggregates were composed of the β-II but not of the β-III spectrin subunit.

DISCUSSION
Saitsu *et al*[4] recently showed that in-frame deletion (p.E2207del) or duplication (p.R2308_M2309dup) in the C-terminal region of SPTAN1 causes a specific syndrome characterized by severe ID, IS, hypomyelination, and brain atrophy.[4] We describe here a novel in-frame deletion in the same domain (p.Q2202del). The phenotype of the patient with this mutation (patient-2) overlaps with that of the previously described patients with in-frame C-terminal SPTAN1 mutations, although being milder. For instance, all three patients showed severe ID, but patient-2 was less impaired than the others. Moreover, the previously described patients presented early in life with IS, and their course was characterized by intractable seizures. In contrast, patient-2 did not show IS and his seizures were well controlled with a single antiepileptic drug. Finally, MRI studies revealed pontocerebellar atrophy in all three patients with the in-frame mutations but patient-2 did not show atrophy of other structures or hypomyelination, like the others.

All three in-frame mutations induced the aggregation of the α-II with the β-II and β-III spectrin subunits in primary neuronal cells, suggesting that they have a dominant–negative effect. Although the spectrin aggregation profile associated with p.Q2202del was similar to